Doctoral Dissertation (Censored)

博士論文（要約）

Towards the creation of an ideal Bose gas in a Bose-Fermi mixture

(ボース・フェルミ混合系における理想ボース気体の生成に向けて)

A Dissertation Submitted for the Degree of Doctor of Philosophy

December 2020

令和２年１２月博士（理学）申請

Department of Physics, Graduate School of Science,

The University of Tokyo

東京大学大学院理学系研究科物理学専攻

CHEN YIPING

陈 一枰

Abstract

The ideal Bose gas is the most common model in quantum statistics. It predicts a pure statistical Bose-Einstein condensate (BEC). However, real systems are interactive. Many properties of the BEC are known to be altered by the interaction. Interestingly, the model for interacting BEC is not explicitly connected to the ideal one. One distinctive difference between an interacting BEC and an ideal BEC is that they are in different universality classes. Thus, possess different critical exponents.

Previous investigations on the critical phenomena of interacting BECs all show good agreement with the 3D-XY model, which is predicted to be the universality class for an interacting BEC. But a BEC phase transition which matches the description of the ideal gas model has never been observed.

In this thesis, ^{7}Li bosons are cooled using ^{6}Li fermionic coolant. In addition, the interaction between the bosons is controllable via the Feshbach resonance by changing an external magnetic field applied to the system. This potentially allow us to eliminate the interaction between the bosons to create an equilibrium ideal Bose gas in canonical ensemble under proper condition.

The condition for the Bosons to become non-interacting is experimentally decided in this research. We further consider the possible effects of the Bose-Fermi mixture on the Bosons and find that the Fermions can be treated as simple coolant for our experiment conditions. We also present the method we use to extract precise local information via the inverse Abel transform. We then use this method to examine the equivalence of ensembles, where it is shown that the equilibrium state of the gas is the same with or without the coolant. These results imply that the non-interacting Bose gas created in our system is a close analogue to the ideal Bose gas. Finally, we use both the non-interacting gas and a repulsively interacting gas to measure the isothermal compressibility near the critical point of the BEC phase transition. We find that the scaling behavior is similar in both cases and deviates from the ideal gas model. The deviation matches the interacting 3D-XY model so that we conclude the interacting model offers a better description for the phenomenon. Our results also imply the possible absence of a “textbook” ideal matter wave BEC inside an ultracold atomic gas with tunable interaction.

Contents

Chapter 1

Introduction

Bosons are particles that follow Bose-Einstein statistics who possess integer spin. A key feature of the bosons is the existence of the Bose-Einstein condensate (BEC). BEC is originally predicted by Bose and Einstein in 1920s [*Bose 1924, Einstein 1925*]. BEC describes the phenomenon where macroscopic occupation of the ground state appears near the zero temperature. At first, the BEC was only predicted for non-interacting ideal systems, but has been later extended to include particle interactions, consequently making BEC considered as a generic phenomenon [*Dalfovo 1999, Leggett 2001*]. The interacting BEC theory is mainly discussed at zero temperature and becomes much more complicated in finite temperatures [*Andersen 2004, Proukakis 2008*]. In general, the interacting BEC theory exists some degree of disconnections either in principle or in property with the ideal Bose gas [*Zagrebnov 2001, Yukalov 2016*].

The experimental realization of BEC was achieved much later than the theoretical proposal. In 1995, BEC was finally produced with laser cooling and trapping techniques using rubidium [*Anderson 1995*], sodium [*Davis 1995*] and lithium atoms [*Bradley 1995*]. Atomic BEC possess much more degrees of freedom on various parameters such as the spin state, density, and even interacting strength compared to traditional strongly interacting liquid helium. Therefore, atomic BEC has since been used to study quantum physics in a relatively simple and controllable manner. Up until now, numerous researches have been conducted using the ultracold atomic gas exploring topics like coherency [*Andrews 1997*], collective excitations [*Jin 1996*], Mott insulator [*Greiner 2002*], Josephson junction [*Albiez 2005*], Efimov effect [*Kraemer 2006*], and Anderson localization [*Roati 2008*]. Advanced trapping and controlling techniques are also invented such as optical lattices [*Jaksch 1998, Morsch 2006*], optical tweezer [*Gustavson 2002*], artificial gauge potentials [*Dalibard 2011*], and box trap [*Gaunt 2013*]. With the recent advancement in the idea called quantum simulation [*Georgescu 2014, Horikoshi 2019, Altman 2019*], BEC is shown to be able to simulate other phenomena such as high-harmonic generation [*Feng 2019*] and quantum gravity [*Howl 2019*, *Hu 2019*].

1.1 Bose Einstein condensate

BEC describes a state of matter, and the process for thermal atoms to enter the condensate state is a kind of second-order phase transition. From the ideal gas model this is simply a result of statistics. For interacting gases this can be understood that the gauge U(1) symmetry of the

thermal particles is broken during the transition.

In a real experimental system, the generation of BEC has some notable features. First, it takes place at a finite temperature and therefore is a classical phase transition. However, the boundary between classic and quantum can be obscure for such a low temperature. Second, although theoretically BEC can form without any interaction, a real gas possesses interaction. Third, it is usually trapped in inhomogeneously. Last, it involves dynamics.

The earliest experiments on BEC's thermodynamics were conducted using rubidium atoms [*Ensher 1996*] and sodium atoms [*Mewes 1996*], where they measured the condensate fraction's dependence on temperature as well as the critical temperature. Later these properties have been measured for many other systems, ^{7}Li BEC immersed in a cloud of ^{6}Li fermionic atoms [*Schreck 2001a*], which shares a close theme with our experiment. Also, some thermodynamical properties have been measured for the Bose gas using a set of defined global variables [*Shiozaki 2014*, *Poveda-Cuevas 2015*].

One major difference between laboratory BEC and the ideal gas theory is the interaction. The theoretical efforts to include interactions into condensed systems began some 70 years ago by Bogoliubov [*Bogolubov 1947*] and others [*Penrose 1956*] mainly focusing on zero temperature properties, which were later extended to finite temperatures by Lee, Huang and Yang [*Lee 1957*]. Furthermore, the interaction between particles in atomic gases can be tuned via Feshbach resonance in experiments [*Inouye 1998, Courteille 1998*], which is also a powerful tool for atomic ultracold experiments.

Interactions bring about many distinctive effects on BEC in many ways [*Smith 2016*], for instance, alternation in excitation modes [*Jin 1997, Chevy 2002*], chemical potential [*Meppelink 2010*], and the emergence of a quantum depletion [*Lopes 2017*]. It has been pointed out that interactions can change the temperature dependence of BEC [*Giorgini 1996*]. In experiments, the effect of interactions on the critical temperature was measured in 2004 [*Gerbier 2004*] and has been thoroughly examined later [*Smith 2011*]. Another distinct feature is that for interacting BEC, a lack of saturation in the excited sates has been presented [*Tammuz 2011*].

Most produced BECs have repulsive interactions but attractive BECs also exist. In fact, one of the three earliest experiments on BEC features an attractive interaction [*Bradley 1995*]. The ability to tune the scattering length via a Feshbach resonance enables creation of attractive BEC with other species [*Cornish 2000, Lepoutre 2016*]. The attractive BECs have some distinctive properties such as collapse [*Bradley 1997*] and multiple solitons [*Strecker 2002*]. Attractive force can also be used to form a state called quantum droplet [*Cabrera 2018*] and has also been examined using bright soliton [*Cheiney 2018*].

Dynamical behavior is also a very interesting topic. Typically, dynamics can be observed using non-destructive imaging such as partial-transfer absorption [*Ramanathan 2012*], Faraday imaging [*Kristensen 2017*], and shadowgraph imaging [*Wigley 2016*]. The first dynamical BEC

experiment focusing on BEC growth was published in 1998 [*Miesner 1998*]. Some recent experiments include collective emission [*Clark 2017*], prethermal dynamics [*Eigen 2018*], granulation [*Nguyen 2019*] and pattern formation [*Zhang 2020*].

Also, laboratory BEC is a trapped system with a finite size. The existence of the trap alters the property of particles from a free gas. The trap geometry can reduce BEC's dimensionality that will affect BEC's properties [*Petrov 2000, Druten 1997*], which can be experimentally realized [*Görlitz 2001*]. In addition, a two-dimensional phase transition [*Hadzibabic 2008*], the Berezinskii-Kosterlitz-Thouless phase transition, has also been realized using BEC [*Hadzibabic 2006, Fletcher 2015*].

One important result from statistical physics is the scaling theory. It characterizes the properties of a second order phase transition with exponential scaling laws that is irrelevant to the details of the system. A collection of systems with the same set of critical exponents is called a universality class. The scaling theory is a very powerful tool to describe a vast variety of different systems. Interestingly, ideal BEC and interacting BEC belongs to different universality classes. For interacting BEC, measurements on the critical behavior of BEC has been experimented with the correlation length [*Donner 2007*]. In addition, dynamical scaling defined by Kibble-Zurek mechanism [*Zurek 1996, Campo 2014*] has also been measured in BEC [*Weiler 2008, Lamporesi 2013, Navon 2015, Chen 2019*].

Previous experiments on the critical scaling of BEC all showed good agreement with the 3D-XY model, which is the universality class that interacting BEC belongs to [*Stanley 1999, Pelissetto 2002*]. This brings us the curiosity that how the phase transition will change when we remove the interaction, which is the main motivation of this thesis. However, normally we cannot casually create a non-interacting Bose gas in thermal equilibrium. The assistance of an external heat bath is required, which is achieved using sympathetic cooling in a Bose-Fermi mixture.

1.2 Sympathetic cooling and Bose-Fermi mixture

In a mixture of two-component gases that are in thermal contact, the method to cool down one component through elastic collisions with the other pre-cooled component is called sympathetic cooling. One advantage of this method is that it does not rely on the self-interactions of the target component as long as it stays in thermal contact with the coolant. This method is potentially possible to create arbitrarily weak interacting and even non-interacting BEC. The sympathetic cooling was first employed in cold atom experiments with a mixture of two hyperfine states of ^{87}Rb Bose gas [*Myatt 1997*]. In 2001, Hulet group [*Truscott 2001*] and Salomon group [*Schreck 2001b*] demonstrated two experiments of the sympathetic cooling of the bosonic ^{7}Li and the fermionic ^{6}Li.

The first Bose-Fermi superfluid mixture is achieved in 2014 with a mixture of ^{7}Li and ^{6}Li [*Ferrier-Barbut 2014*]. Our system is the second one to create such a mixture. In our system, when the magnetic field is tuned to 832 G, i.e., the Feshbach resonance of ^{6}Li, there exist two boson BEC components after cooling, one being repulsively interacting and the other being attractive. Furthermore, the zero crossing of the scattering length for the attractive component is not far from 832 G. This species is used to generate a non-interacting Bose gas in this thesis.

Recently, Bose-Fermi superfluid mixtures of ^{6}Li-^{41}K [*Yao 2016*], ^{6}Li-^{174}Yb [*Roy 2017*] and ^{6}Li-^{133}Cs [*DeSalvo 2017*] have also been realized. Unique phenomena such as phase separation [*Lous 2018*], breathing mode [*Huang 2019*] and induced interaction [*DeSalvo 2019*] have also been examined.

1.3 Motivations and aims

Thus far, research on the Bose gas and BEC has been mostly focused on the repulsively interacting regime and weakly attractive regime. Though some experiments explored the non-interacting BEC regime by changing the interaction using the BEC, a non-interacting ideal Bose gas at finite temperature has not been examined. In the thermal regime, a non-interacting Bose gas cannot thermalize on its own, thus a finite temperature non-interacting Bose gas in equilibrium is only obtainable via sympathetic cooling. While it is known that certain disconnections might exist between ideal gas model and weakly interacting model, they have not been thoroughly examined. More specifically, it is not experimentally known how the critical behavior of interacting BEC approaches the ideal gas behavior when we decrease the interaction.

The first aim of this thesis is to create a non-interacting Bose gas as close as possible towards a “textbook” description of the ideal Bose gas. To achieve this, we have to first find the non-interacting condition, and then verify the effect of the mixture and ensure that the existence of the coolant does not change the properties of the Bose gas. Once we have created such a representation, we aim to explore its critical behaviors by measuring the isothermal compressibility, which is the only accessible quantity to obtain the critical scaling with current set-up. We will also conduct the same experiment using interacting gas and compare their results to the ideal Bose gas model.

1.4 Thesis outline

This thesis is organized as follows:

Chapter 2 gives a brief introduction to the theory of Bose gas. Including the ideal gas model,

the interacting model, and the scaling theory.

Chapter 3 is an introduction of our experimental set-up. Including laser cooling and trapping processes, the Feshbach resonance and the imaging systems. We also demonstrate how the experimental parameters are measured.

Chapter 4 shows our experimental results of the scattering length measurement where we change the external magnetic field and locate the non-interacting condition for the bosons using the ground state of the condensate.

Chapter 5 discusses the effects of the Bose-Fermi mixture on bosons such as mixability, induced potential and induced interaction. We also present related experimental results.

Chapter 6 presents how the equation of state is measured from absorption images and demonstrates the violation of the local density approximation in BEC. The temperature measurement results that are used in later chapters is also shown.

Chapter 7 discusses the concept of the three ensembles and the equivalence or potential differences between them. We estimate the relations between the ensembles to establish a connection between our experiment, other ultracold atom experiments and the textbook case.

Chapter 8 explains how the isothermal compressibility is measured from the equation of state. We present our experimental results with the repulsive gas and non-interacting gas where the critical behaviors are identified in both cases. The possible implications of the results are also discussed.

Chapter 2

Backgrounds of the Bose gas

2.1 Ideal Bose gas

Non-interacting bosons, who can occupy any available energy level with any number and are indistinguishable, satisfy the following relation under the framework of the grand canonical ensemble in thermodynamic equilibrium

$$f(\varepsilon_i) = \frac{1}{e^{(\varepsilon_i - \mu)/k_B T} - 1}, \tag{2.1}$$

where k_B is the Boltzmann constant, ε_i is the energy of state *i*, and μ is the chemical potential. This equation is the well-known Bose-Einstein distribution. The chemical potential is defined by the total particle number *N* so that

$$N = \sum_i f(\varepsilon_i). \tag{2.2}$$

Evidently, the distribution on any energy level must be non-negative for equation (2.1) to make sense. For the lowest level, which is set to be zero, we have the following relation

$$n_0 = f(0) = \frac{1}{e^{-\mu/k_B T} - 1}. \tag{2.3}$$

When the temperature approaches zero, we must have $\mu < 0$ to make this equation meaningful. Under such a condition, any excited state become unoccupied as

$$\frac{n_a}{n_0} = \frac{e^{-\mu/k_B T} - 1}{e^{(\varepsilon_a - \mu)/k_B T} - 1} \leq \frac{e^{-\mu/k_B T}}{e^{(\varepsilon_a - \mu)/k_B T}} = e^{-\varepsilon_a/k_B T} \xrightarrow{T \to 0} 0, \tag{2.4}$$

$$n_0 = \frac{1}{e^{-\mu/k_B T} - 1} \xrightarrow{T \to 0} N. \tag{2.5}$$

This result directly indicates that macroscopic occupation occurs at zero temperature and all the particles “condensated”. This phenomenon is called the Bose-Einstein condensate (BEC).

If the ideal Bose gas is confined in a box of volume *V*, we can write the single-particle Hamiltonian as

$$H_{(1)} = \frac{p^2}{2m}. \tag{2.6}$$

The solutions of this Hamiltonian under cyclic boundary conditions $\varphi(x, y, z) = \varphi(x + L, y, z)$ and the same with the other two direction, where $L = V^{1/3}$, takes the form of plane waves

$$\varphi_p = \frac{1}{\sqrt{V}} e^{i\vec{p}\cdot\vec{r}/\hbar}, \tag{2.7}$$

where $\vec{p} = 2\pi\hbar\vec{n}/L$ and $\vec{n} = (n_x, n_y, n_z)$ is a vector with integer components. The number of thermal atoms then can be written as

$$N_T = \sum_{p\neq 0} \frac{1}{e^{p^2/2m-\mu} - 1} = \frac{V}{\lambda_{dB}^3} \mathrm{Li}_{3/2}\left(e^{\beta\mu}\right), \tag{2.8}$$

where $\beta = 1/(k_B T)$. The thermal de Broglie wavelength is defined as

$$\lambda_{dB} = \sqrt{\frac{2\pi\hbar^2}{mk_B T}}. \tag{2.9}$$

The Bose function is defined as

$$\mathrm{Li}_p(z) = \frac{1}{(p-1)!}\int_0^\infty dx x^{p-1} \frac{1}{z^{-1}e^x - 1} = \sum_{l=1}^{\infty} \frac{z^l}{l^p}, \tag{2.10}$$

where we have introduced the fugacity $z = \exp(\beta\mu)$. By setting the particle density $n = N/V$, equation (2.8) gives the equation of state of the thermal Bose gas

$$n = \frac{1}{\lambda_{dB}^3} \mathrm{Li}_{3/2} e^{\beta\mu}. \tag{2.11}$$

The local critical temperature of a trapped thermal Bose gas can be found by setting the chemical potential to the ground state

$$T_c^0 = \frac{2\pi\hbar^2}{mk_B}\left(\frac{n}{\zeta(3/2)}\right)^{\frac{2}{3}} = \frac{2\pi\hbar^2}{mk_B}\left(\frac{n}{2.612}\right)^{\frac{2}{3}}, \tag{2.12}$$

where ζ is the Riemann zeta function. Below the critical temperature, we can write the total atom number as $N = N_0 + N_T$, where N_0 is the number of condensate atom. This gives us the relation between condensate fraction and temperature

$$\frac{N_0^{\mathrm{uni}}(T)}{N} = 1 - \left(\frac{T}{T_c}\right)^{3/2}. \tag{2.13}$$

In our experiment system, the atoms are trapped in a harmonic form external potential

$$V(\vec{r}) = \frac{m}{2}\left(\omega_x^2 x^2 + \omega_y^2 y^2 + \omega_z^2 z^2\right). \tag{2.14}$$

The eigenenergies of the Hamiltonian take the form

$$\varepsilon_{n_x n_y n_z} = \left(n_x + \frac{1}{2}\right)\hbar\omega_x + \left(n_y + \frac{1}{2}\right)\hbar\omega_y + \left(n_z + \frac{1}{2}\right)\hbar\omega_z. \tag{2.15}$$

In this case the ground state energy is no longer zero. By setting the critical chemical potential to the ground state energy, we can define the global critical temperature and condensate fraction

$$T_{cg}^0 = \frac{\hbar\omega_{ho}}{k_B}\left(\frac{N}{\zeta(3)}\right)^{1/3} = 0.94\frac{\hbar\omega_{ho}}{k_B} N^{1/3}, \tag{2.16}$$

$$\frac{N_0(T)}{N} = 1 - \left(\frac{T}{T_c^0}\right)^3, \tag{2.17}$$

where the geometric average of the oscillator frequencies is defined as

$$\omega_{ho} = \left(\omega_x \omega_y \omega_z\right)^{1/3}. \tag{2.18}$$

Note that the condensate fraction is modified comparing to the uniform case equation (2.13).

The discussion above is based purely on quantum statistics and does not consider interaction. Therefore, ideal BEC can be considered as the result of inherent statistical nature of the bosons.

2.2 s-wave scattering length

The strength of interaction in ultracold physics are usually characterized with the scattering length. The most common form of scattering is the s-wave scattering. Let us first consider a simply scattering problem of two free particles under a hard-sphere potential with diameter a. Their two-body wave function are given by

$$\Psi(\vec{r}_1, \vec{r}_2) = e^{i\vec{P}\cdot\vec{R}}\psi(\vec{r}), \tag{2.19}$$

where

$$\begin{aligned} \vec{R} &= \frac{1}{2}(\vec{r}_1 + \vec{r}_2), \\ \vec{r} &= \vec{r}_2 - \vec{r}_1. \end{aligned} \tag{2.20}$$

We can consider the interaction as boundary conditions and view the particles as free, hence their Schrödinger equation becomes

$$\begin{aligned} \left(\nabla^2 + k^2\right)\psi(\vec{r}) &= 0 \quad (r > a), \\ \psi(\vec{r}) &= 0 \quad (r \le a). \end{aligned} \tag{2.21}$$

Let us restrict ourselves to the spherically symmetric (s-wave) and low energy ($k \to 0$) part. The equation is broken into a radial one

$$\frac{1}{r^2}\frac{d}{dr}\left(r^2 \frac{d\psi}{dr}\right) = 0 \quad (r > a). \tag{2.22}$$

Then, the solution outside the hard-sphere is

$$\psi(r) = \text{const.}\left(1 - \frac{a}{r}\right) \quad (r > a). \tag{2.23}$$

In order to obtain the exact behavior outside the sphere, we need to modify the hard-sphere boundary condition by extending the free Schrodinger equation inside the sphere

$$\left(\nabla^2 + k^2\right)\psi(r) = 0 \quad (r \ne 0), \tag{2.24}$$

with the boundary condition

$$\psi(a)=0. \tag{2.25}$$

For low energy limit $k\to 0$, we have

$$\psi(r)\xrightarrow{r\to 0}\left(1-\frac{a}{r}\right)\chi, \tag{2.26}$$

where χ is a constant related to the boundary condition at $r=\infty$, we can also write

$$\chi=\left[\frac{\partial}{\partial r}(r\psi)\right]_{r=0}. \tag{2.27}$$

Then we can inspect the behavior of equation (2.24) near $r=0$

$$\nabla^2\psi(r)\xrightarrow{r\to 0}4\pi a\delta(\vec{r})\chi=4\pi a\delta(\vec{r})\frac{\partial}{\partial r}(r\psi). \tag{2.28}$$

Hence, we can write a new equation that is satisfied everywhere

$$\left(\nabla^2+k^2\right)\psi(r)=4\pi a\delta(\vec{r})\frac{\partial}{\partial r}(r\psi). \tag{2.29}$$

We can see that the r.h.s. of this equation functions as a kind of contact potential (pseudopotential). However, equation (2.29) does not provide the exact result, by expanding the wave function in spherical harmonics and repeating the process above, one can obtain the exact equation for the pseudopotential

$$\left(\nabla^2+k^2\right)\psi(r)=\frac{4\pi}{-k\cot\delta_0}\delta(\vec{r})\frac{\partial}{\partial r}(r\psi)+\text{higher partial waves terms}, \tag{2.30}$$

where δ_0 is the phase shift that can be expanded by

$$\frac{4\pi}{-k\cot\delta_0}=4\pi\frac{\tan ka}{k}=4\pi a\left[1+\frac{1}{3}(ka)^2+\cdots\right]. \tag{2.31}$$

By taking low energy s-wave limit, Equation (2.30) reduces to Equation (2.29). With such a potential, the large distance behavior of the wave function, namely the asymptotic wave function, can be described as (see Fig. 2.2.1.)

$$r\psi_\infty(r)\equiv\lim_{r\to\infty}r\psi(r)=\text{const.}(\sin kr+\tan\delta_0\cos kr), \tag{2.32}$$

where only a phase shift takes place compared with free gas. In a low energy s-wave scattering, the relation between the induced phase shift and the scattering length takes a simple form

$$a=-\frac{1}{k\cot\delta_0}. \tag{2.33}$$

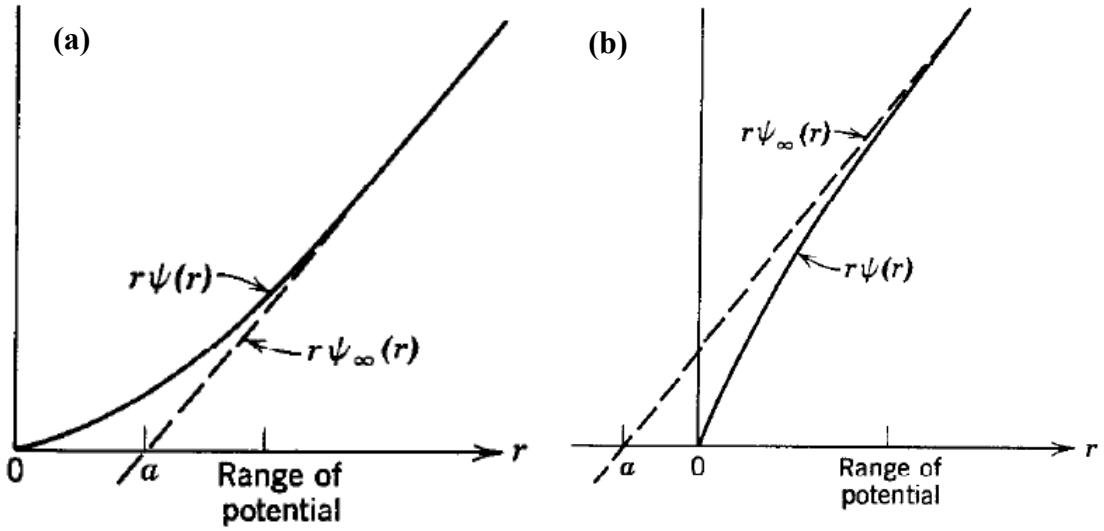

Fig. 2.2.1. The effect of scattering on the wave function with **(a)** a positive scattering length (repulsive) and **(b)** a negative scattering length (attractive). The scattering length is the intercept of the asymptotic wave function with the *x* axis. The repulsive or attractive effects can be seen intuitionally. Taken from [*Huang 1987*].

2.3 The Gross-Pitaevskii equation

The Gross-Pitaevskii (GP) equation serves as the interacting model for the Bose gas at zero temperature. The second-quantized Hamiltonian to describe a system of N interacting bosons trapped inside an external potential can be written as

$$\begin{aligned}\hat{H} = &\int d^3\vec{r}\,\hat{\Psi}^\dagger(\vec{r})\left[-\frac{\hbar^2}{2m}\nabla^2 + V_{\text{ext}}(\vec{r})\right]\hat{\Psi}(\vec{r}) \\ &+\frac{1}{2}\int d\vec{r}d\vec{r}'\hat{\Psi}^\dagger(\vec{r})\hat{\Psi}^\dagger(\vec{r}')V_{\text{int}}(\vec{r}-\vec{r}')\hat{\Psi}(\vec{r}')\hat{\Psi}(\vec{r}).\end{aligned} \tag{2.34}$$

In the s-wave scattering case, the interacting potential can be treated as a pseudopotential similar to equation (2.29)

$$V_{\text{int}}(\vec{r}-\vec{r}') = g\delta(\vec{r}-\vec{r}'), \tag{2.35}$$

where the coupling constant is written with the s-wave scattering length

$$g = \frac{4\pi\hbar^2 a}{m}. \tag{2.36}$$

Using the commutation relations

$$\begin{aligned}\left[\hat{\Psi}(\vec{r}'),\hat{\Psi}^\dagger(\vec{r})\right] &= \delta(\vec{r}'-\vec{r}) \\ \left[\hat{\Psi}(\vec{r}'),\hat{\Psi}(\vec{r})\right] &= \left[\hat{\Psi}^\dagger(\vec{r}'),\hat{\Psi}^\dagger(\vec{r})\right] = 0.\end{aligned} \tag{2.37}$$

We can obtain the Heisenberg equation for the field

$$\begin{aligned} i\hbar\frac{\partial\hat{\Psi}(\vec{r},t)}{\partial t} &= \left[\hat{\Psi}(\vec{r}),\hat{H}\right] \\ &= \left[-\frac{\hbar^2}{2m}\nabla^2 + V_{\text{ext}}(\vec{r}) + g\hat{\Psi}^{\dagger}(\vec{r},t)\hat{\Psi}(\vec{r},t)\right]\hat{\Psi}(\vec{r},t). \end{aligned} \tag{2.38}$$

Since at zero temperature macroscopic occupation occurs, we can decompose the Bose field operator into a mean field term

$$\psi(\vec{r},t) \equiv \left\langle\hat{\Psi}(\vec{r},t)\right\rangle, \tag{2.39}$$

and a fluctuation term

$$\hat{\Psi}(\vec{r},t) = \psi(\vec{r},t) + \hat{\Psi}'(\vec{r},t). \tag{2.40}$$

This is called the mean field approach. Now we can simply drop the fluctuation term and equation (2.38) becomes the Gross-Pitaevskii equation

$$i\hbar\frac{\partial}{\partial t}\psi(\vec{r},t) = \left(-\frac{\hbar^2}{2m}\nabla^2 + V_{\text{ext}} + g\left|\psi(\vec{r},t)\right|^2\right)\psi(\vec{r},t), \tag{2.41}$$

Note that the classic field ψ also severs the roll of an order parameter since the one-particle density matrix

$$\rho_1(\vec{r}',\vec{r},t) = \left\langle\hat{\Psi}^{\dagger}(\vec{r}',t)\hat{\Psi}(\vec{r},t)\right\rangle, \tag{2.42}$$

satisfies the following off-diagonal long-range behavior

$$\lim_{|\vec{r}'-\vec{r}|\to\infty}\rho_1(\vec{r}',\vec{r},t) = \psi^*(\vec{r}',t)\psi(\vec{r},t). \tag{2.43}$$

The Gross-Pitaevskii equation can be calculated easily and is widely used in both theoretical works and experiments. It provides precise estimation of the BEC at zero temperature.

2.4 Weakly interacting gas at finite temperature

When one attempts to extend the theory of an interacting Bose gas to finite temperature, things become much more difficult. How one should model such a system is still an ongoing topic for theorists. A review of this topic is given in [*Proukakis 2008*] where they summarized various methods developed to describe the interacting system. Here we will only summarize the basic idea.

The Hamiltonian of an interacting system equation (2.34) can be decomposed by writing the field operator into two parts

$$\hat{\Psi}(\vec{r},t)=\phi(\vec{r},t)+\delta(\vec{r},t), \tag{2.44}$$

where $\hat{\phi}$ is the field operator for the condensate and $\hat{\delta}$ is the field operator for the thermal atoms. Since the condensate state is macroscopically occupied, the $\hat{\phi}$ is replaced using the condensate wavefunction $\phi(\vec{r},t)=\sqrt{N_0}\varphi_0(\vec{r},t)$, this is called the Bogoliubov approximation. Then we can write down the decomposed Hamiltonian as

$$\hat{H}=H_0+\hat{H}_1+\hat{H}_2+\hat{H}_3+\hat{H}_4, \tag{2.45}$$

where

$$\begin{aligned}
H_0&=\int d\vec{r}\left[\phi^*\hat{h}_0\phi+\frac{g}{2}|\phi|^4\right],\\
\hat{H}_1&=\int d\vec{r}\left[\hat{\delta}^\dagger\left(\hat{h}_0+g|\phi|^2\right)\phi+\phi^*\left(\hat{h}_0+g|\phi|^2\right)\hat{\delta}\right],\\
\hat{H}_2&=\int d\vec{r}\left[\hat{\delta}^\dagger\left(\hat{h}_0+2g|\phi|^2\right)\hat{\delta}+\frac{g}{2}\left(\left(\phi^*\right)^2\hat{\delta}\hat{\delta}+\phi^2\hat{\delta}^\dagger\hat{\delta}^\dagger\right)\right],\\
\hat{H}_3&=g\int d\vec{r}\left[\phi\hat{\delta}^\dagger\hat{\delta}^\dagger\hat{\delta}+\phi^*\hat{\delta}^\dagger\hat{\delta}\hat{\delta}\right],\\
\hat{H}_4&=\frac{g}{2}\int d\vec{r}\hat{\delta}^\dagger\hat{\delta}^\dagger\hat{\delta}\hat{\delta},\\
\hat{h}_0&=\frac{-\hbar^2}{2m}\nabla^2+V_{\text{ext}}(\vec{r}).
\end{aligned} \tag{2.46}$$

This Hamiltonian can be calculated by omitting one or several terms or taking further approximations. This results in various models, which are generally created to address certain problems. Typically, the modeling process gets more problematic as the temperature increases when the condensate atoms become lesser. In a general sense, there is no existing calculatable perfect model to solve all the problems for an interacting Bose gas and it is not explicitly connected to the ideal gas model.

2.5 Scaling theory

The scaling theory describes the properties of a system near the critical point of a second-order phase transition. Here we use the Landau-Ginsburg theory to introduce some basic concepts. Near the critical point of the phase transition, the free energy density of the system takes the form

$$\psi\left(m(x),H(x)\right)=\frac{1}{2}\left|\nabla m(x)\right|^2+\frac{1}{2}r_0m^2(x)+u_0m^4(x)-\frac{1}{k_BT}m(x)H(x), \tag{2.47}$$

where $m(x)$ is the order parameter, H is an external field, and u_0 and r_0 are some detailed parameters. The phase transition occurs when r_0 reaches zero

$$r_0 = a_0 \varepsilon, \qquad \varepsilon = \frac{T - T_c}{T_c}, \tag{2.48}$$

where a_0 is another detailed parameter. A schematic of the free energy near the critical point is shown in Fig. 2.5.1.

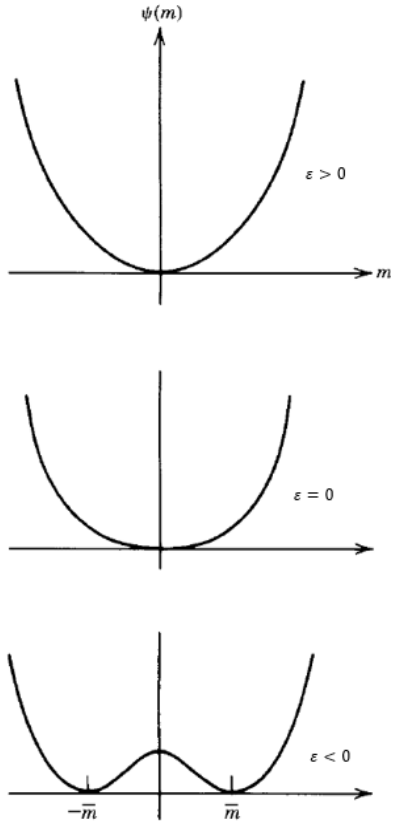

Fig. 2.5.1. The free energy near a second-order phase transition. The order parameter appears when $\varepsilon < 0$. $\varepsilon = 0$ is where the phase transition occurs and is called the critical point. Taken from [*Huang 1987*].

We will use the spatial correlation of the system as an example. This property can be examined by introducing a test source

$$H(x) = -\lambda \delta(x). \tag{2.49}$$

The free energy influenced by this source then becomes

$$E[m] = \int dx \left[-\frac{1}{2} m \nabla^2 m + \frac{1}{2} r_0 m^2 + u_0 m^4 + \lambda m(x) \delta(x) \right], \tag{2.50}$$

and we can obtain the corresponding differential equation

$$\left[\nabla^2 - r_0 - 4u_0 m^2(x) \right] m(x) = \lambda \delta(x). \tag{2.51}$$

This equation can be solved by taking Fourier transforms

$$\tilde{m}(k)=\frac{\lambda}{k^2+r_0},\quad \bar{m}(x)=\lambda\int(dk)\frac{e^{ikx}}{k^2+r_0}\xrightarrow{x\to\infty}x^{2-d}e^{-x/\xi}. \tag{2.52}$$

Then the correlation length can be found to be

$$\xi=\begin{cases}(r_0)^{-1/2}\\(-2r_0)^{-1/2}\end{cases}=\begin{cases}(a_0\varepsilon)^{-1/2} & (\varepsilon>0),\\(-2a_0\varepsilon)^{-1/2} & (\varepsilon<0).\end{cases} \tag{2.53}$$

We can see that the reaction of the order parameter to a certain fluctuation is spatially correlated near the critical point, which can be characterized with an exponent. Therefore, we can obtain the critical exponent of correlation length ν as

$$\xi\sim\varepsilon^{-\nu}=\varepsilon^{-1/2}. \tag{2.54}$$

Apparently, this critical exponent is irrelevant of all the detailed parameters. It can be shown that all other critical exponents also share this property, which is a key feature of the scaling theory. Also note that this form of Landau mean field scaling is only quantitatively correct for systems with at least four spatial dimensions.

Similarly, we can calculate the critical exponents for all kinds of realistic systems. But since the scaling is irrelevant to the microscopic details of a system, it simply reflects the scale invariance which the system possesses in the vicinity of the critical point. That is to say, empirically lots of systems can be found obeying the same critical scaling, as shown in Fig. 2.5.2. The collection of systems that share a same set of critical exponents is called a universality class. The universality classes are known to be only dependent on some few properties of the systems: the dimension of the system, the dimension of the order parameter and the range of interaction.

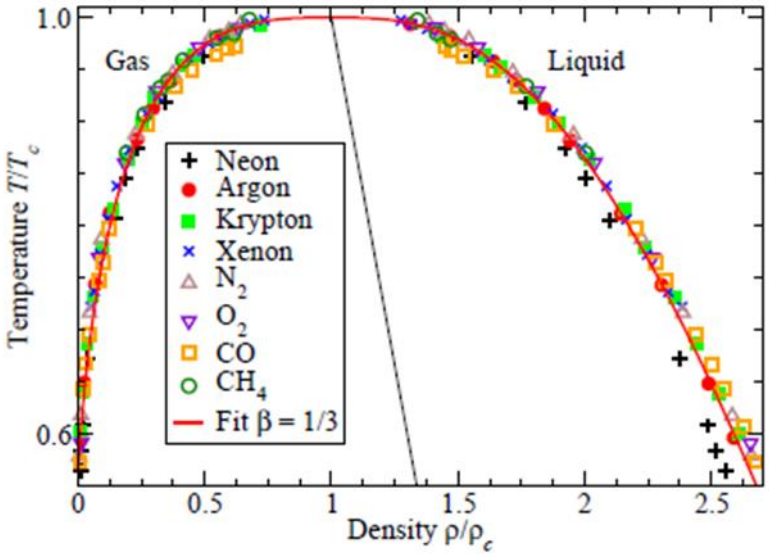

Fig. 2.5.2. The universality in the Gas-liquid coexistence region. Taken from [*Sethna 2006*].

For ideal gas, since we already know the partition function, all thermodynamic properties can be strictly calculated. A detailed discussion for all the critical exponents can be found at Chapter 13 of [*Pathria 2011*]. They show that the universality class for the ideal BEC coincides with the spherical model, which corresponds to the $n \to \infty$ limit of a *n*-vector model [*Stanley 1999*]. Here we are interested in the isothermal compressibility which is defined as

$$\kappa_T = \frac{1}{n^2}\frac{\partial n}{\partial \mu}\bigg|_T . \tag{2.55}$$

The exact expression for the isothermal compressibility can be obtained from equation (2.8), which is

$$\kappa_T^{\text{ideal}} = \frac{1}{n^2 \lambda_{dB}^3 k_B T}\,\text{Li}_{1/2}\left(e^{\beta\mu}\right). \tag{2.56}$$

This value obeys the scaling law

$$\kappa_T^{\text{ideal}} \sim \varepsilon^{-1}. \tag{2.57}$$

For interacting gas, ideally one may also derive all the critical exponents from the partition function. However, the problem is that we do not know the exact expression for the partition in this case. Generally speaking, one might as well construct an effective action $S[\phi; \mathrm{g}]$, where ϕ is a field and g is a vector of coupling constants $\mathrm{g} = (\mathrm{g}_1, \mathrm{g}_2, \mathrm{g}_3, \cdots)$, to express the partition function Z as

$$Z(g) = \int D[\phi] e^{-S[\phi;g]}, \tag{2.58}$$

where $\int D[\phi] = \prod_{i=1}^{N} \int (dx_i/\sqrt{2\pi})$ in *N*-dimension. Then, we can apply the Wilsonian renormalization group method to evaluate the critical exponents. The first thing we would like to do is to decompose the field in the momentum space into slow modes $\phi^<$ and fast modes $\phi^>$ written as $\phi = \phi^< + \phi^>$ so that we can get rid of the large field part

$$\begin{aligned} Z(g) &= \int D\left[\phi^<\right] \int D\left[\phi^>\right] e^{-S\left[\phi^< + \phi^>; g\right]} \\ &= \int D\left[\phi^<\right] e^{-S_\Lambda^<\left[\phi^<; g^<\right]}. \end{aligned} \tag{2.59}$$

After this mode elimination, we will rescale the system in terms of rescaled quantities where the quantities retain the same form as before. This operation is possible for that the system is scale invariant, i.e., self-similar near the critical point. The rescaled wave vector is defined as

$$k' = bk, \tag{2.60}$$

where *b* is the step size of the renormalization group transformation. Then the rescaled field $\phi'(k')$ can be written using the original field $\phi^<(k')$ as

$$\phi'(k') = \zeta_b^{-1} \phi^<(k'/b), \tag{2.61}$$

where $\zeta_b = b^{D_\phi}\sqrt{Z_b}$ is called the field rescaling factor. The factor D_ϕ is the canonical

dimension of the field that measures the powers of inverse length needed to make it dimensionless. The factor Z_b is called the wave function renormalization factor and can be chosen based on the need of the calculation.

Combining the mode-elimination and the rescaling steps, one can obtain a mapping for the initial coupling $\mathrm{g} = (\mathrm{g}_1, \mathrm{g}_2, \mathrm{g}_3, \cdots)$ with initial action $S[\phi; \mathrm{g}]$ and a set of modified coupling $\mathrm{g}' = (\mathrm{g}_1', \mathrm{g}_2', \mathrm{g}_3', \cdots)$ with the effective action $S'[\phi'; \mathrm{g}']$, expressed via

$$\begin{aligned} g_i' &= R_i\left(b; g_1, g_2, g_3, \cdots\right), i = 1, 2, 3, \cdots \\ &\rightarrow g' = \mathbf{R}(b; g). \end{aligned} \tag{2.62}$$

The renormalization group transformation function **R** is usually in complex nonlinear form. By iterating these two processes, we obtain a chain of renormalized couplings

$$g^{(n)} = \mathbf{R}(b; g^{(n-1)}) = \mathbf{R}(b^n; g). \tag{2.63}$$

Then, by analyzing how the properties changes during these operations, we can numerically evaluate the critical exponents. The techniques involved in actual renormalization group calculations are vastly complicated and one might find a thorough introduction in, e.g., [*Kopietz 2010*].

The scaling law for the isothermal compressibility of the interacting gas can be calculated using the renormalization group method in 3DXY model, which gives [*Campostrini 2006*]

$$\kappa_T^{3\mathrm{DXY}} \sim \varepsilon^{-1.3}. \tag{2.64}$$

Note that the this result is different from the ideal gas model equation (2.57), showing some degree of disconnection.

Chapter 3

Experimental set-up

The experimental set-up of our experiment includes two separate laser systems for ^{6}Li and ^{7}Li and a trapping system composed of a 2D magneto-optical trap, a 3D magneto-optical trap and two optical dipole traps. We will present the details of our set-up and showcase how the experimental parameters are measured.

3.1 Laser cooling

The idea of laser cooling is based on the scattering process between photon and atom. When a moving atom absorb a photon, its speed changes according to the momentum of the photon. Therefore, when we apply a laser beam in the opposite direction of a moving beam of atoms, we can ideally decelerate the atoms. However, things are far more complicated in real world due to the doppler effect. If moving in the same direction, the angular frequency of the laser ω in the stationary frame is changed to $\omega' = \omega - kv$, where v is the speed of atom and $k = 2\pi/\lambda$ is the wavevector of the light, or $\omega' = \omega + \omega v/c$ if moving in opposite direction.

When a laser beam is incident towards a moving atom, the scattering force the atom received is estimated by the number of photons absorbed, that is, $F_{\mathrm{sc}} = (\mathrm{Momentum}) \times (\mathrm{Scattering\ rate})$. With a certain amount of detune δ, this scattering force can be written as

$$\begin{aligned} R_{\mathrm{sc}} &= \frac{\Gamma}{2}\frac{I/I_{\mathrm{sat}}}{1+I/I_{\mathrm{sat}}+(2\delta/\Gamma)^2}, \\ F_{\mathrm{sc}} &= \hbar k\frac{\Gamma}{2}\frac{I/I_{\mathrm{sat}}}{1+I/I_{\mathrm{sat}}+(2\delta/\Gamma)^2}, \end{aligned} \tag{3.1}$$

where R_{sc} is the scattering rate, Γ is the absorption line width, I is the laser intensity and I_{sat} is the saturation intensity. The maximum amount of deceleration the atom with mass m receives is

$$a_{\mathrm{max}} = \frac{\hbar k}{m}\frac{\Gamma}{2}. \tag{3.2}$$

Typically, the atom with initial velocity v_0 stops in a distance of $L_{\mathrm{stop}} = v_0^2/a_{\mathrm{max}}$.

The atom species used in our set-up are ^{6}Li and ^{7}Li. The level structure of these atoms is shown in Fig 3.1.1. The two species are cooled by separate lasers. For ^{6}Li the D2 line from the ground state $|F = 3/2\rangle$ to the excite state $|F' = 5/2\rangle$ is used to cool down the atom, where the laser beam is labeled as “cooling” laser. For ^{7}Li the D2 line $|F = 2\rangle \rightarrow |F' = 3\rangle$ is used. Ideally the “cooling” laser alone is sufficient to cool down the atoms, however, the energy

difference between the highest hyperfine state of $2P_{1/2}$ and the lowest hyperfine state of $2P_{3/2}$ is very small. Therefore, occasionally the atoms will enter $2P_{1/2}$ and relaxed to the ground state $|F = 1/2\rangle$ for ^{6}Li or $|F = 1\rangle$ for ^{7}Li, which then stops to interact with the "cooling" laser. To address this matter, an additional "repump" laser is introduced to pump the atoms from D1 line $|F = 1/2\rangle \rightarrow |F' = 3/2\rangle$ for ^{6}Li and D2 line $|F = 1\rangle \rightarrow |F' = 2\rangle$ for ^{7}Li, which ensures that the atoms are relaxed to the correct ground state and continue the cooling cycle.

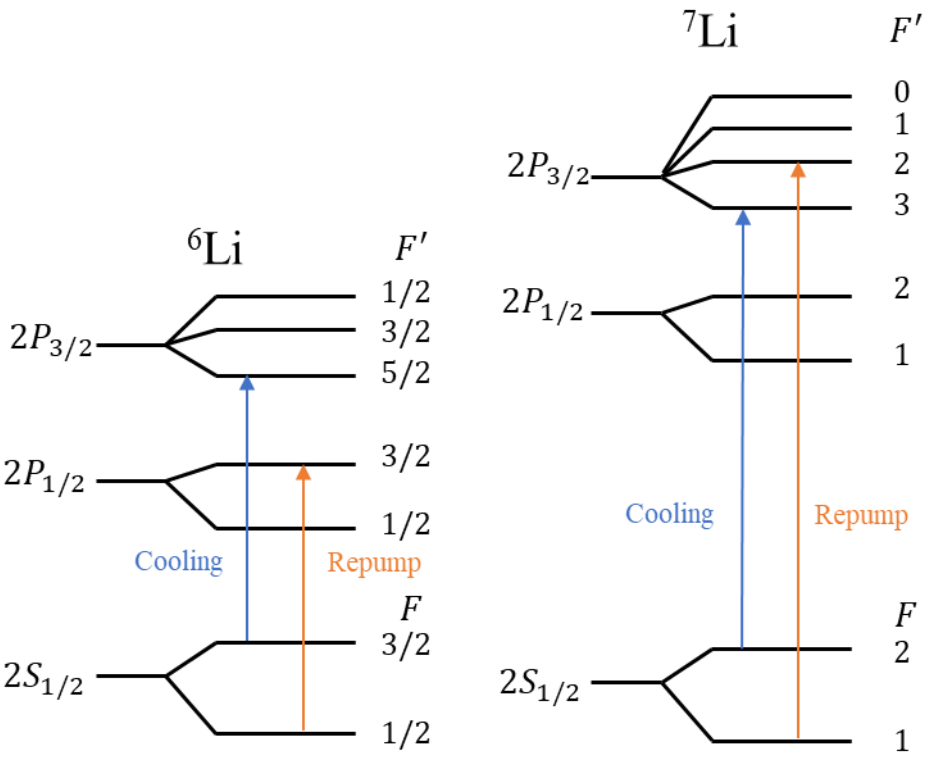

Fig. 3.1.1. Fine level structure of ^{6}Li and ^{7}Li.

We use GaAs diode laser as source of external cavity diode laser (ECDL) to obtain single frequency laser beam. The locking processes of the lasers are based on the saturated absorption spectroscopy of the ^{6}Li $|F = 3/2\rangle \rightarrow |F' = 5/2\rangle$ D2 line, where an oven with ^{6}Li inside is heated to about 360 ℃ to provide atom source. After this ^{6}Li "cooling master" laser is locked, it serves as the base frequency for all other lasers. The ^{6}Li "repump" laser is locked by applying a 9.8 GHz offset locking and ^{7}Li "cooling" laser is also locked with a 10.3 GHz offset locking. The ^{7}Li "repump" laser is set by tuning its "cooling" laser for 800 MHz with an acousto-optic modulator (AOM).

The detuning introduced by the Doppler effect reduces the absorption and consequently prevents us to cool down the atoms. There are two common solutions to the Doppler shift problem, one by manipulating the laser, another by manipulating the atoms. The first one is

called the chirp cooling which is achieved by scanning the frequency of the laser. The method we adopt here is the later one using Zeeman effect by applying a magnetic field.

3.2 Magneto-optical trap

The magneto-optical trap (MOT) is invented to slow down and trap the atoms at the same time. When a magnetic field that is linear to position $\vec{B} = B'\vec{r}$ is applied, where the zero point is the center of the trap, the detuning that an atom feels is modified to $\delta' = \delta - \vec{k}\cdot\vec{v} + \mu_B\left|\vec{B}\right|/\hbar$. The last term corresponds to Zeeman shift where μ_B is the magnetic moment of the atom. For simplicity we first consider a 1D case. Inside this field, two laser beams are applied in the opposite direction, then the scattering force on an atom from each side is

$$\begin{aligned}\vec{F}_{\pm} &= \pm\frac{\hbar\vec{k}\Gamma}{2}\frac{I/I_{\text{sat}}}{1+I/I_{\text{sat}}+(2\delta_{\pm}/\Gamma)^2},\\ \delta_{\pm} &= \delta \mp \vec{k}\cdot\vec{v} \pm \frac{\mu_B\left|\vec{B}\right|}{\hbar}.\end{aligned} \tag{3.3}$$

The total scattering force on this atom then becomes

$$\vec{F}_{\text{MOT}} = \vec{F}_{+} + \vec{F}_{-} \approx \frac{8\hbar k^2\delta\left[\vec{v}-\vec{r}\mu_B B'/(\hbar k)\right]I/I_{\text{sat}}}{\Gamma\left[1+I/I_{\text{sat}}+\left(2\delta/\Gamma\right)^2\right]^2}. \tag{3.4}$$

This force can be separated in terms of velocity and position

$$\vec{F}_{\text{MOT}} = -\beta_{\text{MOT}}\vec{v} - \kappa_{\text{MOT}}\vec{r}, \tag{3.5}$$

It is obvious that this force provides a damped oscillation to the atom and traps the atom around the center. The trap can be optimized by adjusting the laser detuning δ and the slope of the magnetic field B'. If we apply this method in two dimensions, the trap is called a 2D magneto-optical trap (2D-MOT). If applied to all dimensions, it is called a 3D magneto-optical trap (3D-MOT).

In our set-up, the trap system is separated into a low-vacuum chamber and a high-vacuum chamber that is connected via a differential pumping tube, as shown in Fig. 3.2.1. This double-chamber set-up ensures a high-quality vacuum environment for the observation, which is vital in cold atom experiments. In the low-vacuum chamber, a beam of ^{6}Li and ^{7}Li coming out from an oven heated to about 320 ℃ is ejected towards a 2D-MOT. The atoms pre-cooled from the 2D-MOT then continue to propagate through the differential pumping tube to the high-vacuum chamber and are trapped inside a 3D-MOT. The purpose of pre-cooling the atoms with a 2D-MOT before trapping is to reduce the presence of high temperature atoms which will decrease the trap lifetime through scattering during subsequent processes. Typically, around 2×10^8

^{6}Li and 2×10^8 ^{7}Li at a temperature on the order of 1 mK are collected after a capture period of 40 second.

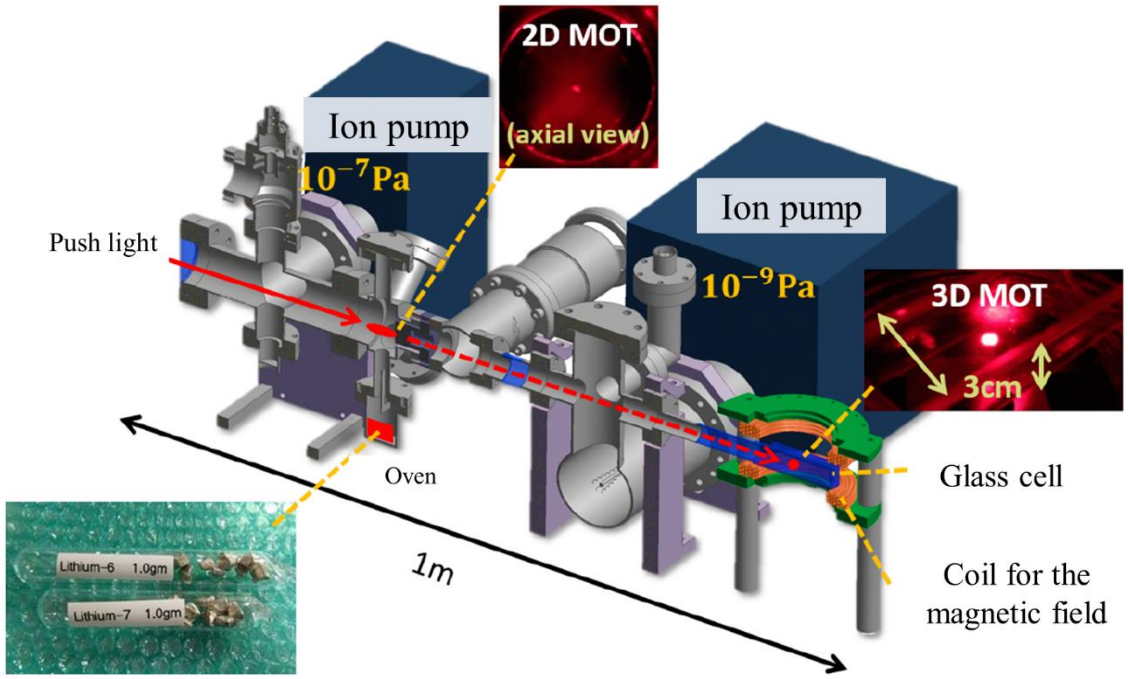

Fig. 3.2.1. A schematic view of the MOT.

Since laser cooling excites an atom, recoil from spontaneous emission causes the atom to change its velocity into random directions. Although this kick from recoil is averaged to zero, it triggers a random walk effect on the atoms, which prevents them from further cooling. The severity of the random walk is related to the steps taken, which is decided by the scattering rate in this case. The mean square velocity resulting from this effect in a single direction from a single laser beam is $\overline{v_{\text{spon}}^2} = \hbar k R_{\text{sc}} t/(3m)$ within a time period of t. Meanwhile, the fluctuations raised from the number of absorptions within this period will also add another random walk velocity with similar form $\overline{v_{\text{abs}}^2} = \hbar k R_{\text{sc}} t/m$. For a 3D-MOT, the total mean square velocity from the random walk in equilibrium can be calculated from the Newton equation, which can be translated into a related temperature written as

$$k_B T = \frac{\hbar\Gamma}{4} \frac{1+(2\delta/\Gamma)^2}{-2\delta/\Gamma}. \tag{3.6}$$

The minimum can be found at $\delta = -\Gamma/2$, which is

$$k_B T_D = \frac{\hbar\Gamma}{2}. \tag{3.7}$$

This temperature T_D is known as the Doppler cooling limit. For our system this value is about 140 μK. In order to further cool down the gas, sub-Doppler cooling is required.

3.3 Optical dipole trap

In our set-up the atoms are transferred to an optical dipole trap (ODT) for sub-Doppler cooling. For an atom with polarizability $\epsilon_0\chi$, an electric field $\vec{E}$ induces a dipole moment of $-e\vec{r} = \epsilon_0\chi\vec{E}$. Then the interaction energy between this dipole with the field when the detune is much larger than the line width can be written as [*Grimm 2000*]

$$U_{\text{dip}}(\vec{r}) = -\frac{1}{2}e\vec{r}\cdot\vec{E} = -\frac{3\pi c^2\Gamma}{2\omega_0^3}\left(\frac{\Gamma}{\omega_0-\omega}+\frac{\Gamma}{\omega_0+\omega}\right)I(\vec{r}), \tag{3.8}$$

where ω_0 is the resonant angular frequency and Γ is the absorption line width of the two-level structured atom. For a Gaussian beam of

$$\begin{aligned} I(\vec{r}) &= \frac{2P}{\pi w(z)^2}e^{-2\frac{\vec{r}^2}{w(z)^2}}, \\ w(z) &= w_0\sqrt{1+\left(\frac{z}{z_R}\right)^2}, \end{aligned} \tag{3.9}$$

where P is the power of the beam, w_0 is the beam waist, and $z_R = \pi w_0/\lambda$ is the Rayleigh length. This dipole interaction is attractive and cylindrically symmetric. In the regime close to the focus, the potential takes a harmonic form

$$\begin{aligned} U_{\text{dip}}(\vec{\rho}) &= -U_0 + \frac{m\omega_r r^2}{2} + \frac{m\omega_z z^2}{2}, \\ U_0 &= \frac{3c^2P}{w_0^2\omega_0^3}\left(\frac{\Gamma}{\omega_0-\omega}+\frac{\Gamma}{\omega_0+\omega}\right), \\ \omega_r &= \sqrt{\frac{4U_0}{mw_0^2}},\ \omega_z = \sqrt{\frac{2U_0}{mz_R^2}}. \end{aligned} \tag{3.10}$$

Since the size of the ODT is smaller than the 3D-MOT, we will first shrink the 3D-MOT by adjusting the laser frequency and intensity for a smooth transition. After holding the atoms in this compressed-MOT (CMOT) for 45 ms, roughly 1×10^7 ^{6}Li and 3×10^6 ^{7}Li eventually enter the ODT.

The actual set-up for ODT is depicted in Fig. 3.3.1. The light source is provided by a 200 W, 1070 nm ytterbium fiber laser. The source is separated into two paths to form a high power ODT (HP-ODT) and a low power ODT (LP-ODT). The atoms are first transited into the HP-ODT and then moved to the LP-ODT after some cooling. This configuration is adopted to reduce heat related effects to optics induced by the high intensity laser source, which gives a better shaped trap during the later processes inside the LP-ODT.

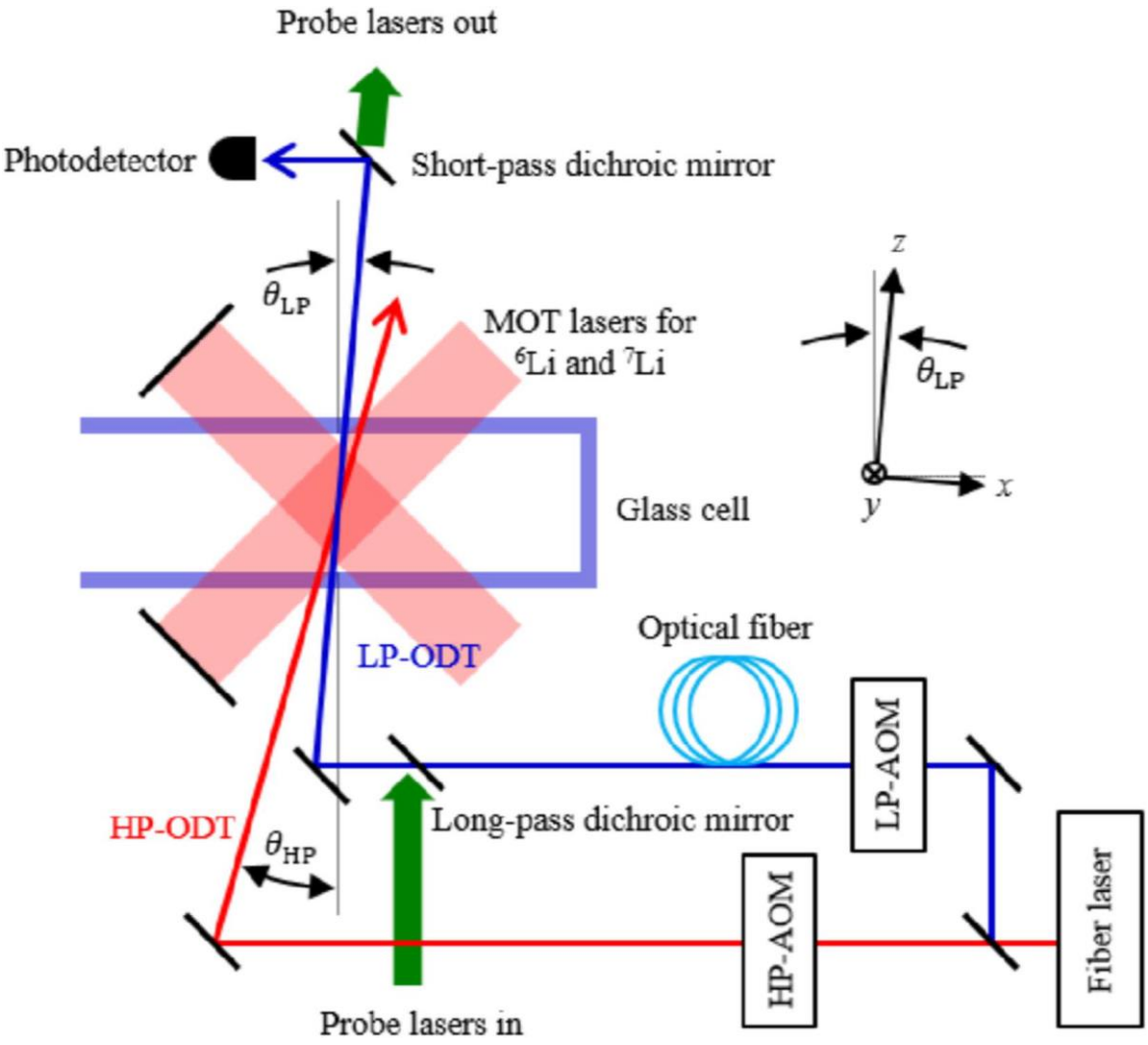

Fig. 3.3.1. The set-up of the optical dipole trap system.

After the atoms are loaded inside the ODT, we apply evaporative cooling to further reduce the temperature. Unlike laser cooling, evaporative cooling is achieved by deducing the laser intensity for the trap. It is known that certain scaling laws exist to minimalize the atom loss and optimize the cooling efficiency [*O'Hara 2001*]. The average energy for the atom lost when we decrease the trap potential can be written as $U_{\text{trap}} + \alpha kT$, where $0 \leq \alpha \leq 1$. The evolution of the total energy E is related to the atom loss rate N' by

$$E' = N'\left(U + \alpha kT\right) + \frac{U'}{U}\frac{E}{2}. \tag{3.11}$$

From the classical limit of the total energy $E = 3NkT$, we have

$$E' = 3NkT' + 3N'kT. \tag{3.12}$$

Combining these two equations gives

$$\frac{N}{N_{t=0}} = \left(\frac{U}{U_{t=0}}\right)^{3/(2\eta'-6)}, \tag{3.13}$$

where $\eta = U_{\mathrm{trap}}/(kT)$ and $\eta' = \eta + \alpha = \eta + (\eta - 5)/(\eta - 4)$. The value of parameter α is estimated with the harmonic potential using the s-wave Boltzmann equation. The loss rate is evaluated to be [*Luiten 1996*]

$$N' = -2(\eta - 4)e^{-\eta}\gamma_{\mathrm{ela}}N, \tag{3.14}$$

where $\gamma_{\mathrm{ela}} \propto Nv^3/(kT)$ is the elastic collision rate. Then, the scaling for the trap depth can be written as

$$\frac{U(t)}{U_{t=0}} = \left(1 + \frac{t}{\tau}\right)^{-2(1-3/\eta')}, \tag{3.15}$$

where constant τ takes the from $1/\tau = 2\eta'(\eta - 4)\exp(-\eta)\gamma_{\mathrm{ela}}^{t=0}/3$. In practice this means that we need to deduce the trap depth according to a specific power law to effectively cool down the gas. The optimization of this scaling has already been done for our set-up in previous experiments.

The evaporative cooling process is separated into three-steps as illustrated in Fig. 3.3.2. The first step takes place after the transition of atoms from CMOT into HP-ODT. This step reduces the trap temperature from 2.8 mK to 560 μK. The second evaporation begins as we turn on the LP-ODT and further reduce the intensity of HP-ODT, the two traps are spatially overlapped so that the atoms are automatically transits into the LP-ODT during this process. The trap temperature in LP-ODT after this process is 38 μK. Then the third step starts in the LP-ODT to further reduce the temperature to the order of 100 nK. The typical number of atoms after a 30 second evaporation is about 3×10^5 ^{6}Li and 5×10^4 for ^{7}Li. The atoms are finally imaged after a small period of holding.

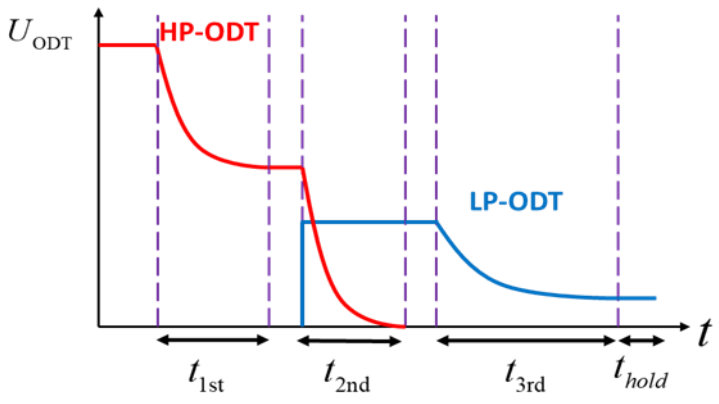

Fig. 3.3.2. A typical three-step evaporation.

As shown in equation (3.15), the efficiency of the evaporative cooling is dependent on the elastic collision rate, which is proportional to the square of scattering length. The scattering length between atoms are controlled by the Feshbach resonance.

3.4 Feshbach resonance

In a low energy scattering, when the scattering energy is close to a bound state, the scattering process becomes resonant, as shown in Fig. 3.4.1. This process is called Feshbach resonance which modifies the interaction strength between atoms. A detailed review of this topic is given in [*Chin 2010*] and here we will only summarize the key features.

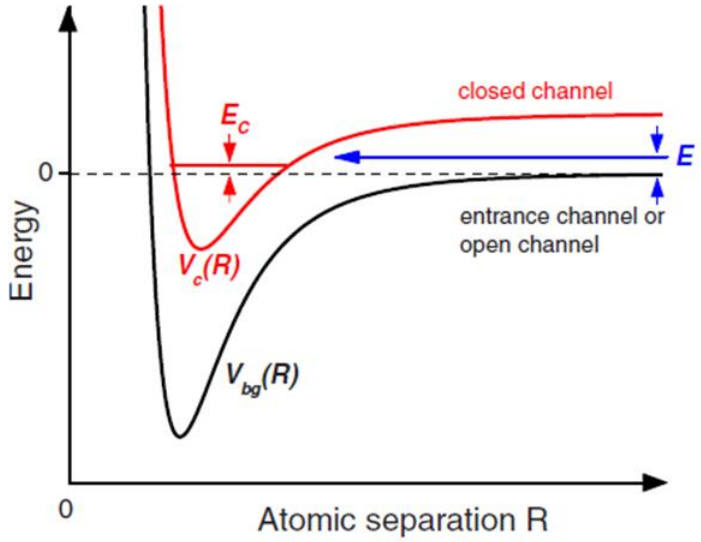

Fig. 3.4.1. The two-channel model of the Feshbach resonance. Resonant interaction is induced when the scattering energy E approaches a bound state energy E_C. V_c and V_{bg} are atom potentials where V_{bg} is fixed and V_c changes with the magnetic field. Taken from [*Chin 2010*].

The initial state configuration of the two atoms is called the entrance channel and the different states which the two can be coupled is called the closed channel. The zero energy in the closed channel can be varied with an external parameter, which is the magnetic field B in our case. The Feshbach resonance can also be induced using radio-frequency or optical radiation. In the magnetic Feshbach resonance case, when the energy of a bound state in the closed channel crosses the scattering energy of the entrance channel, the scattering process gets enhanced resulting in a divergence of scattering length a. The width in magnetic field Δ of this resonance depends on the coupling strength of the two channels. The scattering length effected by all the resonances takes the form

$$a = a_{bg}\prod_i\left(1-\frac{\Delta_i}{\left(B-B_{0,i}\right)}\right), \tag{3.16}$$

where a_{bg} is the background scattering length and B_0 is the resonant magnetic field, the subscript i marks the number of each resonance.

For the purpose of manipulating the scattering length, a bias magnetic field of 832.18 G is applied simultaneously when the CMOT is turned on and remains throughout the evaporative cooling process. The value of this bias magnetic field is adjusted during the second evaporation to a final value between 800 G to 900 G to suit the needs of the experiment. The atom species we use in this thesis are the hyperfine levels of ^{6}Li $|F = 1/2\rangle$ and ^{7}Li $|F = 1\rangle$. The resonance between ^{6}Li $|F = 1/2, m_f = +1/2\rangle$ and $|F = 1/2, m_f = -1/2\rangle$ are located at 832.18 G and is considered to diverge across the whole magnetic regime we examined in this thesis. For this reason, the ^{6}Li fermions cool down extremely fast during the evaporative cooling, typically faster than a scale of tens of milliseconds, and is served as coolant for the ^{7}Li bosons. The interaction between the bosons and the fermions is at a constant value of $a_{bf} \sim 40a_0$ according to [*Ferrier-Barbut 2014*]. This scattering is the responsible for the cooling bosons. The strength of this scattering is large enough for the bosons to cool down in the order of seconds.

For the ^{7}Li bosons, we use either $|F = 1, m_f = -1\rangle$ or $|F = 1, m_f = 0\rangle$. The third hyperfine state $|F = 1, m_f = +1\rangle$ disappears during the first evaporation due to frequent inelastic collision. The other two hyperfine states remain in the trap and we will remove one of them after the second evaporation using the probe laser to avoid mixing these two. The $|F = 1, m_f = 0\rangle$ is used as repulsive gas at 832.18 G, with a scattering length of $a_{00} = 70a_0$ [*Gross 2011*, *Julienne 2014*]. The $|F = 1, m_f = -1\rangle$ is the candidate for the non-interacting gas, where the response of the scattering length to the magnetic field has not been measured before. A rough schematic of the scattering length in a mixture of $|F = 1/2, m_f = +1/2\rangle$ and $|F = 1/2, m_f = -1/2\rangle$ fermions and $|F = 1, m_f = -1\rangle$ bosons is shown in Fig. 3.4.2, the values used to calculate the scattering length is taken from [*Ferrier-Barbut 2016*].

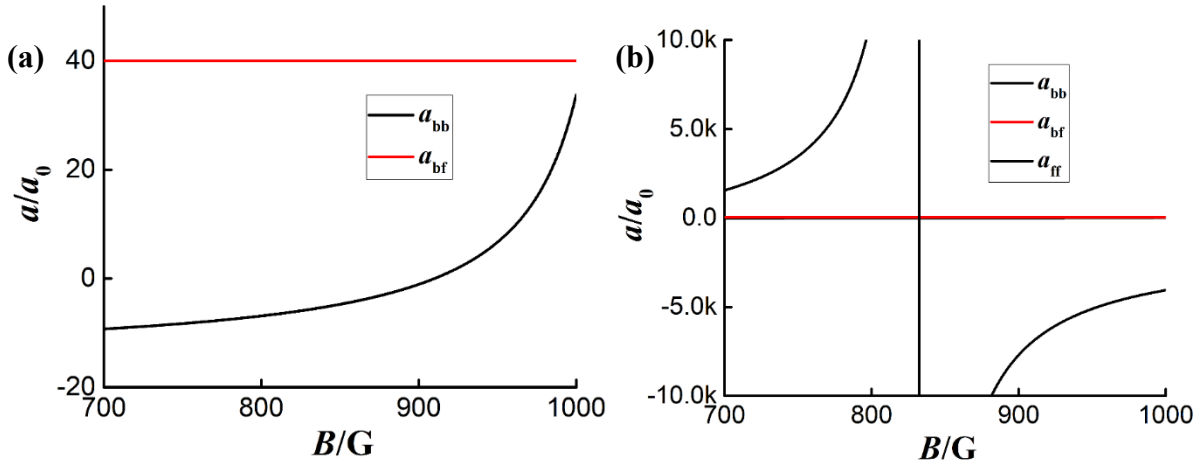

Fig. 3.4.2. The Feshbach resonance of the atoms. **(a)** The scattering length of the bosons (black line) and the scattering length between the bosons and fermions (red line). **(b)** Same as (a), with the scattering length of the fermions added and the vertical axis rescaled.

3.5 Imaging system

The method we obtain information on the ultracold atoms we created is through imaging. The imaging system in our set-up features two probes, one for in-situ absorption imaging and the other for time-of-flight (TOF) imaging. A schematic of the probe system is shown in Fig. 3.5.1. The Cartesian coordinate system for the trap is set as follows: the propagation direction of the ODT laser is the *z* direction, the gravity is in the *y* direction and the horizontal direction vertical to the laser beam is the *x* direction. Some examples of the images taken inside the Bose-Fermi superfluid mixture at 832.18 G is shown in Fig. 3.5.2 [*Ikemachi 2016*]. The pixel size for the in-situ camera is $L_{pix} = 13\ \mu\text{m}$ with a imaging magnification of $M_{mag} = 7.68$, therefore, the size of each pixel in the captured image is $d = L_{pix}/M_{mag} = 1.7\ \mu\text{m}$. The TOF camera has a pixel size of $16\ \mu\text{m}$ and a adjustable imaging magnification between 1 and 3.28. The TOF images from LP-ODT uses a magnification of 3.28 while the lower magnification is used to adjust the 3D-MOT and HP-ODT.

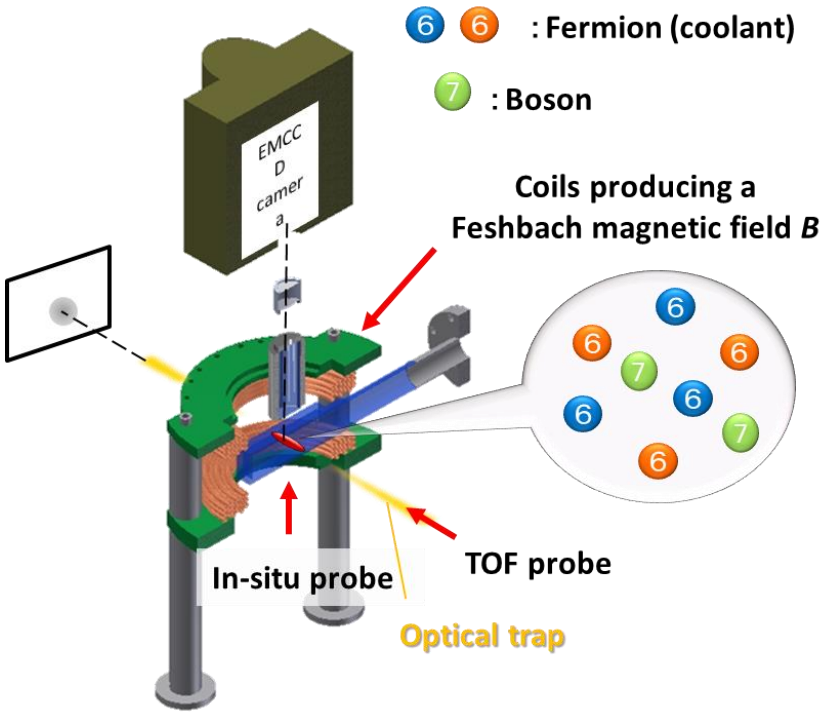

Fig. 3.5.1. A schematic view of the imaging system.

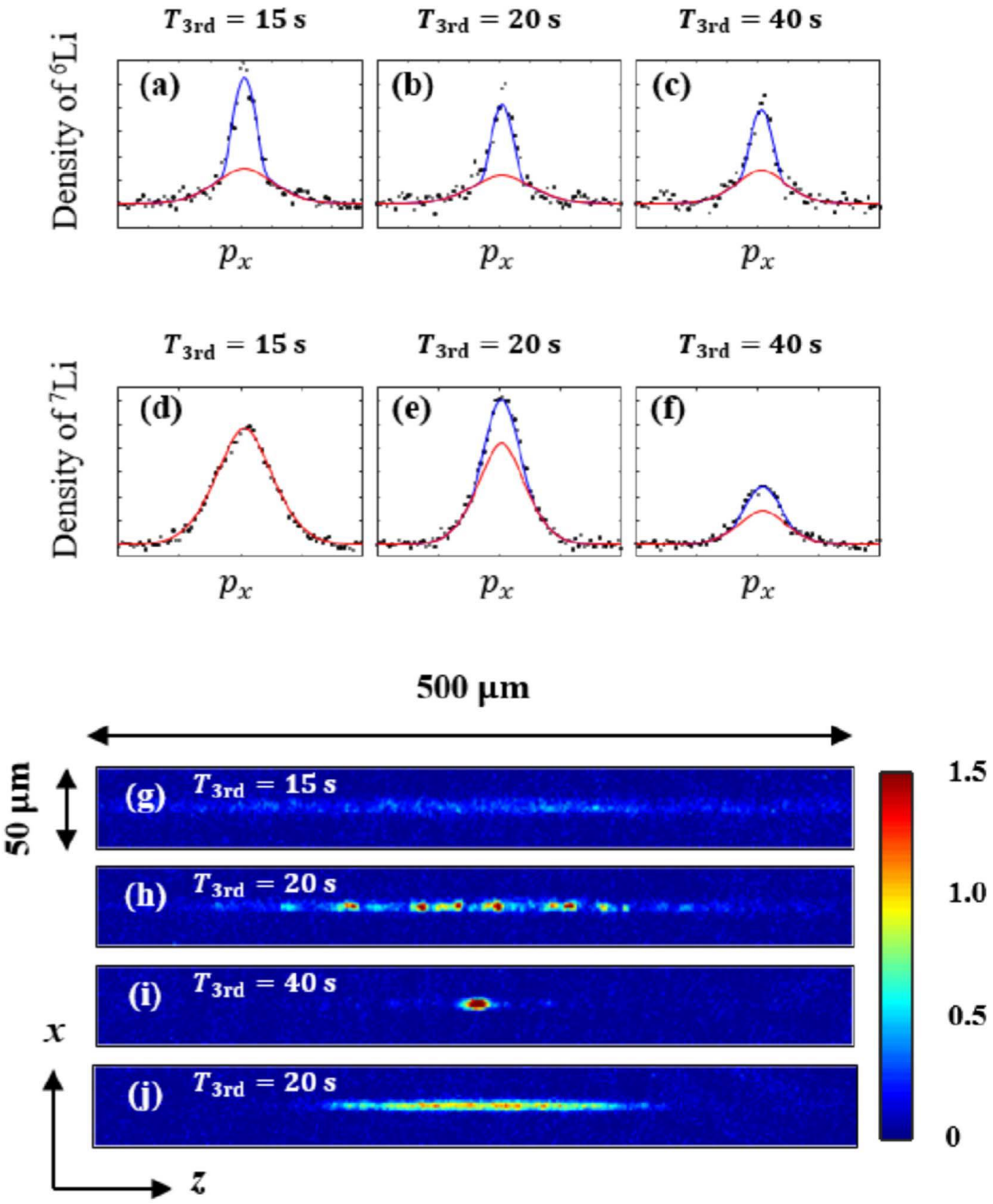

Fig. 3.5.2. Examples of the Bose-Fermi mixture after third evaporation with different cooling time. **(a-c)** The TOF images of paired fermions, black dots are the integrated momentum distributions along the *y* direction and the lines are results of a bimodal fitting. **(d-f)** The TOF images of bosons. **(g-i)** In-situ images of the $|F = 1, m_f = -1\rangle$ boson. **(j)** In-situ image of the $|F = 1, m_f = 0\rangle$ boson.

The TOF probe is set in the same path as the ODT and is mainly used to evaluate the temperature of the atoms. Additionally, it is used to observe the collective oscillation of atoms.

When we are attempting to measure the temperature, the trap is turned off at a designated moment and the atoms enter ballistic movement. The probe is applied after the atoms fly for a period of t, typically about serval milliseconds. The mean square spread of the atoms after this flight can be written as

$$\begin{aligned}\overline{r^2(t)} &= \int dr \int dv r^2 f(r+vt, v) \\ &= \int dr' \int (r'-vt)^2 f(r', v) \\ &= \int dr' \int r'^2 f(r', v) + t^2 \int dr' \int v^2 f(r', v) \\ &= \overline{r^2(0)} + \overline{v^2} t^2,\end{aligned} \tag{3.17}$$

where $f(r, v)$ is the distribution of atoms in the phase space. We can use the Maxwell distribution to evaluate the atoms

$$f(r, v) = C e^{-\frac{r^2}{r(0)^2}} e^{-\frac{v^2}{2\sigma^2}}, \tag{3.18}$$

where σ is connected to the temperature via $\sigma^2 = k_B T/m$. The 1/e value $r(t)$ of the distribution during the flight is

$$r(t) = \sqrt{r(0)^2 + 2(\sigma t)^2}. \tag{3.19}$$

Since the image is taken in strong confinement directions (*x*-*y* plane) the $r(0)$ simply corresponds to the geometric mean of the harmonic frequency of the trap in *x* and *y* directions. Therefore, by fitting the spread after the flight, we can obtain the temperature of the atoms.

The in-situ probe is used to obtain the density distribution of the trapped atoms. This method is called absorption imaging from which the total number of atoms and local density can be calculated. A detailed description is given in [*Horikoshi 2017a*]. When a probe laser with intensity I pass through the atom cloud, its intensity decreases according to the Beer-Lambert law

$$\frac{dI(x, y, z)}{dy} = -n(x, y, z) \frac{\sigma_{\text{abs}}}{1 + \frac{I(x, y, z)}{I_{\text{sat}}}} I(x, y, z), \tag{3.20}$$

where σ_{abs} is the absorption cross section. The column density then can be derived as

$$\bar{n}(x, z) = \frac{1}{\sigma_{\text{abs}}} \left[-\ln\left(\frac{I_{\text{out}}}{I_{\text{in}}}\right) + \frac{I_{\text{in}}}{I_{\text{sat}}} \left(1 - \frac{I_{\text{out}}}{I_{\text{in}}}\right) \right], \tag{3.21}$$

Where $I_{\text{in}}(x, z) = I(x, -\infty, z)$ is the incident intensity and $I_{\text{out}}(x, z) = I(x, +\infty, z)$ is the output intensity. The optical depth (OD) is defined as

$$OD(x, z) = \sigma_{\text{abs}} \bar{n}(x, z). \tag{3.22}$$

In an realistic experimental run, an absorption image is calculated from 3 CCD counting images. The first one is the probe laser with atoms C_{abs}. The second one is the probe laser without atoms C_{probe}. The third one is the background without the probe laser C_{back}. The background is removed as $C_{\mathrm{in}} = C_{\mathrm{probe}} - C_{\mathrm{back}}$ and $C_{\mathrm{out}} = C_{\mathrm{abs}} - C_{\mathrm{back}}$. Then equation (3.21) can be converted into CCD counts

$$\begin{aligned} C_1(i,j) &= OD(x_i, z_j) - \frac{C_2(i,j)}{\chi_{\mathrm{sat}}}, \\ C_1(i,j) &= -\ln\left[\frac{C_{\mathrm{out}}(i,j)}{C_{\mathrm{in}}(i,j)}\right], \\ C_2(i,j) &= \frac{C_{\mathrm{in}}(i,j) - C_{\mathrm{out}}(i,j)}{t}, \end{aligned} \tag{3.23}$$

where (i, j) labels the location of the pixel correspond to (x_j, z_j), t is the duration of the probe and the saturation count is defined by $C_{\mathrm{sat}} = C(I_{\mathrm{sat}}, t) = \chi_{\mathrm{sat}} t$. From this equation we can see that the saturation count χ_{sat} can be determined from the gradient of C_1 to C_2 and can be measured by changing the probe intensity. For this thesis, $\chi_{\mathrm{sat}} = 1050$ is measured and used for the bosons. The absorption cross section σ_{abs} for the bosons can be measured using the ground state of $|F = 1, m_f = -1\rangle$ with a known scattering length of $70a_0$. Since the total number of atoms can be expressed by OD as

$$N = \frac{\sum OD}{\sigma_{\mathrm{abs}}}\left(\frac{L_{pix}}{M_{mag}}\right)^2, \tag{3.24}$$

we can use the N calibrated from Thomas-Fermi approximation to assess the cross section. The cross section is measured to be $\sigma_{\mathrm{abs}} = 8 \times 10^{-14}\ \mathrm{m}^2$.

3.6 Trap evaluation

Since an amount of bias magnetic field is applied in the z direction, the external potential is modified according to

$$U_{\mathrm{ext}}(x,y,z) = U_{\mathrm{dip}}(x,y,z) + U_{\mathrm{mag}}(z), \tag{3.25}$$

Where the magnetic field provides a simple one-dimensional harmonic potential

$$U_{\mathrm{mag}}(z) = \frac{m}{2}\omega_{\mathrm{mag}}^2 z^2. \tag{3.26}$$

The magnetic curvature ω_{mag} is about $\omega_{6\mathrm{mag}} = 2\pi \times 0.24\sqrt{B}$ Hz for the ^{6}Li fermions and $\omega_{7\mathrm{mag}} = 2\pi \times 0.24\eta\sqrt{B}$ Hz for ^{7}Li bosons, where B is in Gauss and $\eta = \sqrt{m_6/m_7}$.

In our system the trap laser is an elliptic Gaussian beam. When can modify equation (3.9)

to describe its intensity

$$I_{\mathrm{ODT}}(x,y,z)=\frac{2P_{\mathrm{ODT}}}{\pi w_x(z)w_y(z)}\exp\left[-2\left(\frac{x^2}{w_x(z)^2}+\frac{y^2}{w_y(z)^2}\right)\right]$$
$$w_i(z)=w_{0i}\sqrt{1+\left(\frac{z}{z_{Ri}}\right)},\ z_{Ri}=\frac{\pi w_{0i}}{\lambda}, \tag{3.27}$$

where i denotes the direction *x* or *y*. The trapping frequencies then can be expressed by

$$U_0=\frac{3c^2P_{\mathrm{ODT}}}{\omega_0^3 w_{0x}w_{0y}}\left(\frac{\Gamma}{\omega_0-\omega}+\frac{\Gamma}{\omega_0+\omega}\right),$$
$$\omega_x=\sqrt{\frac{4U_0}{mw_{0x}^2}},$$
$$\omega_y=\sqrt{\frac{4U_0}{mw_{0y}^2}}, \tag{3.28}$$
$$\tilde{\omega}_z=\sqrt{\frac{U_0}{m}\left(\frac{1}{z_{Rx}^1}+\frac{1}{z_{Ry}^1}\right)},$$
$$\omega_z=\sqrt{\tilde{\omega}_z^2+\omega_{\mathrm{mag}}^2},$$

where $\tilde{\omega}_z$ is the trapping frequency by the ODT and ω_z is the effective trapping frequency in *z* direction. The trapping frequencies for the bosons satisfy $\omega_7=\eta\omega_6$. The power of the LP-ODT P_{ODT} is controlled by a virtual parameter in our operation system denoted as U_{trap}, ranging from 0 to 10. U_{trap} controls the output of the LP-AOM. In this thesis we refer U_{trap} as trap depth and it has linear relations with P_{ODT} and atom temperature.

The trap parameters w_{x0}, w_{y0} and ω_z can be measured either using the fermions alone without loading the bosons or using the bosons in a mixture. However, in a mixture the frequency cannot be measured by fermions for that its low density gives bad signal to noise ratio.

The trap frequency in *x* and *y* direction can be measured using the collective oscillation. In the case of fermions, we use ideal Fermi gas at 527 G. By turning off the LP-ODT for 30 μs and then re-trap the atoms by turning on the LP-ODT again, a collective oscillation along the *x* and *y* direction can be excited. The oscillation is imaged with the TOF camera where the size of the gas is examined. Fig 3.6.1. shows the results of such a measurement. The oscillation frequency of this mode is $2\omega_x$ and $2\omega_y$. With the measured frequency, we can use equation (3.28) to obtain the beam waists w_{0x} and w_{0y}. For bosons, similar measurement is performed using $m_f=0$ at 832.18 G. The oscillation frequency of the collective mode is $\sqrt{5}\omega_x$ and $\sqrt{5}\omega_y$ [*Miyakawa 2000*]. An example of the oscillation is given in Fig. 3.6.2.

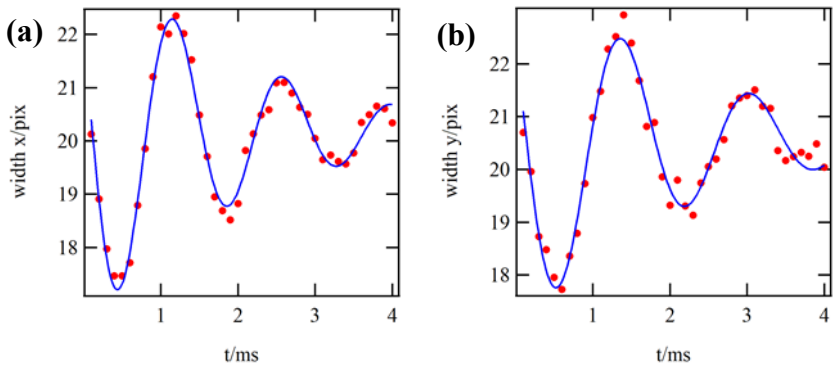

Fig 3.6.1. Example of collective oscillation measured with ideal Fermi gas, $U_{\mathrm{trap}} = 0.40$. **(*a*)** x direction Gaussian width. **(*b*)** y direction Gaussian width. The line corresponds to a sine fit with a lifetime.

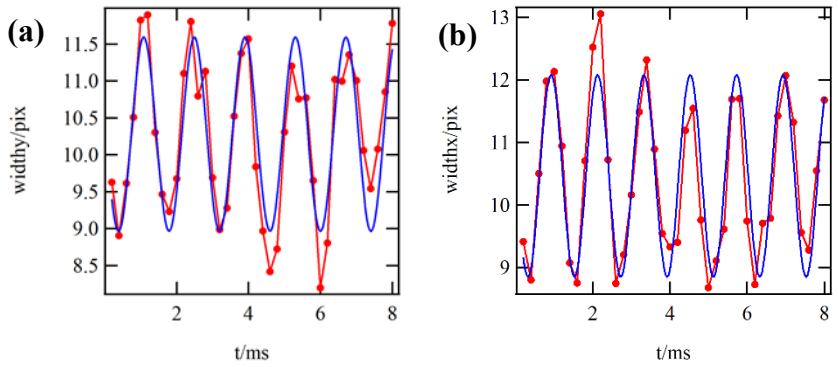

Fig 3.6.2. Example of collective oscillation measured with $m_f = 0$ Bose gas at 832.18 G, $U_{\mathrm{trap}} = 0.50$. **(*a*)** *x* direction Gaussian width. **(*b*)** *y* direction Gaussian width. The line corresponds to a sine fit.

The effective trapping potential ω_z can be measured using the dipole oscillation. The oscillation is excited by briefly turning on the HP-ODT while the atoms are trapped inside the LP-ODT. This provides a modulation in density distribution along the *z* direction which results in a dipole oscillation. In-situ images are taken to evaluate the movement of the center of mass. The oscillation frequency is $1\omega_z$ for both bosons and fermions. Using this measured value and beam waists, we can calculate the magnetic curvature ω_{mag}. An example of the dipole oscillation is shown in Fig. 3.6.3.

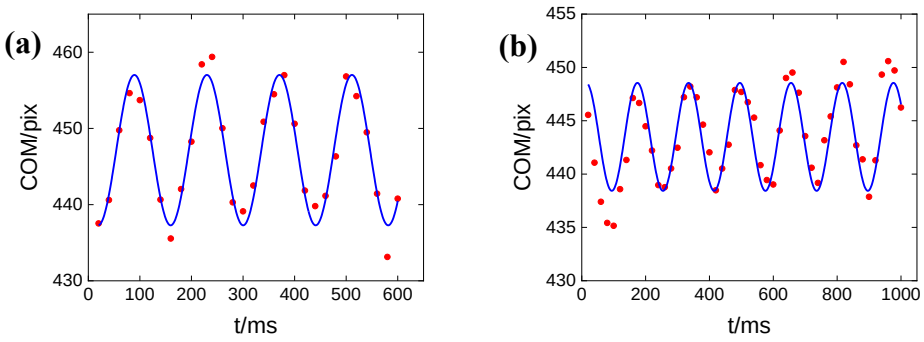

Fig 3.6.3. Example of dipole oscillations evaluated from the movement of center of mass along z direction measured at 832.18 G. **(a)** Fermions at $U_{\mathrm{trap}} = 0.40$. **(b)** Bosons at $U_{\mathrm{trap}} = 0.20$. The line corresponds to a sine fit.

Realistically, the trap parameters can vary slightly based on factors such as the optical path of the ODT and the condition of the fiber laser. The values are found to vary naturally on a weekly to monthly basis in response to environmental changes. Also, the values change during operation compared to that at the start. Therefore, we usually start the experiment after the system has been completely warmed-up when the trap condition as well as the atom loading condition become stabilized. The warm-up operation typically takes around three hours. The changes in trap condition are mostly found in the beam width in x and y direction. However, since these directions are strongly confined and we are mostly dealing with data in the z direction, changes around 1 or 2 μm typically does not affects the result of the experiment. The trapping frequency in z direction is relatively stable because it mainly comes from the magnetic field.

The trap parameters used for the data in Chapter 8 are measured to be $w_{x0} = 40.5$ μm, $w_{y0} = 47.0$ μm, $\omega_{\mathrm{mag}} = 2\pi \times 6.3$ Hz, and $P_{\mathrm{ODT}} = 1.25 * \left(0.642 + 195.13 * U_{\mathrm{trap}}\right)$ mW.

Summary

In this chapter we presented how the Bose gas of ^{7}Li are prepared. We covered the basics of laser cooling, magneto-optical trapping, optical-dipole trapping, evaporative cooling and Feshbach resonance. We also introduced the imaging system and explained how the atom number and density are calculated. Finally, we explained the trap parameters and demonstrated how they are measured.

Conclusion

In this thesis, we have presented the creation of ultracold Bose gases of ^{7}Li using laser cooling, magneto-optical trapping, and optical-dipole trapping. The gas is evaporatively cooled with ^{6}Li coolant to achieve a sympathetic cooling under an external Feshbach magnetic field. We introduced our imaging system and demonstrated how the experimental parameters are determined.

we have measured the scattering length of ^{7}Li bosons in the hyperfine state $|F = 1, m_f = -1\rangle$ across a magnetic field range from 832 G to 900 G via evaluating the size of the ground state BEC. The experimental range covers the scattering length from $-3.2\ a_0$ to $15\ a_0$. We experimentally located the non-interacting limit of the bosons at a magnetic field of 850.5 G, where the scattering length is measured to be $0.08 \pm 0.15\ a_0$. This condition is used to represent an ideal gas.

We examined the properties of the Bose-Fermi mixture which includes mixability, the effects of fermions on the potential of bosons, and the fermion induced interaction between bosons. We find that the boson and fermion components are mixable. The induced potential is found to change the trapping frequency for about 1%. The induced interaction is found to be less than the error of the measured scattering length. Therefore, the effects induced by the mixture can be omitted and the fermions can be treated safely as simple coolant for the bosons.

We presented the calculation of the equation of state where we average more than 30 in-situ absorption images and apply the inverse Abel transform to generate the local density. Then the local density is mapped towards the local potential to obtain the density EOS. We demonstrated the LDA violation in BEC and explained that BEC proportion is removed for isothermal compressible measurement. We also shown the temperature measurement results using TOF imaging and bimodal fitting.

We explored the concept of ensembles and the equivalence between them. We mentioned some under-debate problems regarding the ensembles. We demonstrated that our system composed by bosons and fermionic coolant is equivalent to similar system where bosons are isolated, i.e., the equivalence between canonical ensemble and microcanonical ensemble, by partially removing the heat bath and re-balancing the system. This implies that statistically the experimental results from our system should be the same with the majority of other ultracold atom systems without coolant.

With these results, we can conclude that the non-interacting Bose gas created in our system is a close analogue to the “textbook” case of an ideal Bose gas. We also explained that why such condition can only be obtained via sympathetic cooling.

Finally, we evaluated the local isothermal compressibility for both repulsive Bose gas with $70a_0$ and the non-interacting Bose gas with $0.08 \pm 0.15\ a_0$. We managed to capture this

property by using the inverse Able transform to acquire accurate local information. The gases are found to match the ideal gas model away from the critical point. Similar critical divergence is observed in both cases, where the compressibility deviates the prediction of the ideal gas model and seemingly matches the 3D-XY behavior. The cause for the $0.08a_0$ gas to not following the ideal gas model near critical point can be explained by weakly interacting theory. An ideal BEC phase transition might not be achievable in real experiment conditions since we cannot completely remove all the interaction and the interacting BEC phase transition may be non-perturbatively different from an ideal one. We conclude that interacting model gives a more realistic view of the Bose gas than the ideal model and much care has to be taken for the possible disconnection between these two. Our results also imply the possible absence of a "textbook" ideal matter wave BEC inside an ultracold atomic gas with tunable interaction.

The work in this thesis can be extended in several directions. First, one might consider examine other range of scattering length to locate the existence of a possible crossover between the interacting model and the ideal model. Since we have no idea how exactly the interaction affects the system, the location of this crossover can be very narrow near the effective zero scattering length or somewhere sightly away from it. If one manages to increase the accuracy of the measured critical scaling, one might also be able to identify other possible scenarios such as the Casimir effect. Alternatively, one might use other traps to examine the critical phenomenon, such as a box trap. Although by applying the LDA, the local properties we examined here should be the same with that of a homogenous trap, the harmonic potential changes some global properties of the condensate. Therefore, a box trap should be a closer representation to the textbook case. One might also be interested to examine other possible disconnected properties between the ideal gas and the interacting gas such as the thermal saturation. In addition, thermalization dynamics can be an interesting topic to study, since the temperature range we studied here is somewhere in the vague boundary between quantum and classic.

References

[*Albiez 2005*] M. Albiez, R. Gati, J. Foelling, S. Hunsmann, M. Cristiani, and M. K. Oberthaler, Phys. Rev. Lett. **95**, 010402 (2005).

[*Altman 2019*] E. Altman, *et al.*, arXiv:1912.06938 (2019).

[*Anderson 1995*] M. H. Anderson, J. R. Ensher, M. R. Matthews, C. E. Wieman, and E. A. Cornell, Science **269**, 198 (1995).

[*Andersen 2004*] J. O. Andersen, Rev. Mod. Phys. **76**, 599 (2004).

[*Andrews 1997*] M. R. Andrews, C. G. Townsend, H.-J. Miesner, D. S. Durfee, D. M. Kurn, and W. Ketterle, Science **275**, 637 (1997).

[*Bergeman 2000*] T. Bergeman, D. L. Feder, N. L. Balazs, and B. I. Schneider, Phys. Rev. A **61**, 063605 (2000).

[*Bloch 2000*] I. Bloch, T. W. Hansch, and T. Esslinger, Nature, **403**, 166 (2000).

[*Bogolubov 1947*] N. Bogolubov, J. Phys. (USSR) **11**, 23 (1947).

[*Bose 1924*] S. N. Bose, Z. Phys. **26**, 178 (1924).

[*Bradley 1995*] C. C. Bradley, C. A. Sackett, J. J. Tollett, and R. G. Hulet, Phys. Rev. Lett. **75**, 1687 (1995).

[*Bradley 1997*] C. C. Bradley, C. A. Sackett, and R. G. Hulet, Phys. Rev. Lett. **78**, 985 (1997).

[*Brewczyk 2007*] M. Brewczyk, M. Gajda and K. Rzażewski, J. Phys. B: At. Mol. Opt. Phys. **40**, R1 (2007).

[*Cabrera 2018*] C. R. Cabrera, L. Tanzi, J. Sanz, B. Naylor, P. Thomas, P. Cheiney, and L. Tarruell, Science **359**, 301 (2018).

[*Campa 2009*] A. Campa, T. Dauxois, and S. Ruffo, Phys. Rep. **480**, 57 (2009).

[*Campo 2014*] A. del Campo and W. H. Zurek, Int. J. Mod. Phys. A **29**, 1430018 (2014).

[*Campostrini 2006*] M. Campostrini, M. Hasenbusch, A. Pelissetto, and E. Vicari, Phys. Rev. B **74**, 144506 (2006).

[*Ceccarelli 2014*] G. Ceccarelli and J. Nespolo, Phys. Rev. B **89**, 054504 (2014).

[*Cheiney 2018*] P. Cheiney, C. R. Cabrera, J. Sanz, B. Naylor, L. Tanzi, and L. Tarruell, Phys. Rev. Lett. **120**, 135301 (2018).

[*Clark 2017*] L. W. Clark, A. Gaj, L. Feng, and C. Chin, Nature **551**, 356 (2017).

[*Chan 1988*] M. H. W. Chan, K. I. Blum, S. Q. Murphy, G. K. S. Wong, and J. D. Reppy, Phys. Rev. Lett. **61**, 1950 (1988).

[*Chen 2019*] Y. Chen, M. Horikoshi, K. Yoshioka, and M. Kuwata-Gonokami, Phys. Rev. Lett. **122**, 040406 (2019).

[*Chevy 2002*] F. Chevy, V. Bretin, P. Rosenbusch, K. W. Madison, and J. Dalibard, Phys. Rev. Lett. **88**, 250402 (2002).

[*Chin 2010*] C. Chin, R. Grimm, P. Julienne, and E. Tiesinga, Rev. Mod. Phys. **82**, 1225 (2010).

[*Cornish 2000*] S. L. Cornish, N. R. Claussen, J. L. Roberts, E. A. Cornell, and C. E. Wieman, Phys. Rev. Lett. **85**, 1795 (2000).
[*Courteille 1998*] Ph. Courteille, R. S. Freeland, and D. J. Heinzen, Phys. Rev. Lett. **81**, 69 (1998).
[*Crisanti 2019*] A. Crisanti, A. Sarracino, and M. Zannetti, Phys. Rev. Research **1**, 023022 (2019).
[*Crooker 1983*] B. C. Crooker, B. Hebral, E. N. Smith, Y. Takano, and J. D. Reppy, Phys. Rev. Lett. **51**, 666 (1983).
[*D'Alessio 2016*] L. D'Alessio, Y. Kafri, A. Polkovnikov, and M. Rigol, Adv. Phys. **65**, 239 (2016).
[*Dalfovo 1999*] F. Dalfovo, S. Giorgini, L. P. Pitaevskii, and S. Stringari, Rev. Mod. Phys. **71**, 463 (1999).
[*Dalibard 2011*] J. Dalibard, F. Gerbier, G. Juzeliūnas, and P. Öhberg, Rev. Mod. Phys. **83**, 1523 (2011).
[*Davis 1995*] K. B. Davis, M.-O. Mewes, M. R. Andrews, N. J. van Druten, D. S. Durfee, D. M. Kurn, and W. Ketterle, Phys. Rev. Lett. **75**, 3969 (1995).
[*Delfino 2017*] F. Delfino and E. Vicari, Phys. Rev. A **95**, 053606 (2017).
[*DeSalvo 2017*] B. J. DeSalvo, K. Patel, J. Johansen, and C. Chin, Phys. Rev. Lett. **119**, 233401 (2017).
[*DeSalvo 2019*] B. J. DeSalvo, K. Patel, G. Cai, and C. Chin, Nature **568**, 61 (2019).
[*Desbuquois 2014*] R. Desbuquois, T. Yefsah, L. Chomaz, C. Weitenberg, L. Corman, S. Nascimbène, and J. Dalibard, Phys. Rev. Lett. **113**, 020404 (2014).
[*Diehl 2017*] H. W. Diehl and S. B. Rutkevich, Phys. Rev. E **95**, 062112 (2017).
[*Donner 2007*] T. Donner, S. Ritter, T. Bourdel, A. Öttl, M. Köhl, and T. Esslinger, Science **315**, 1556 (2007).
[*Druten 1997*] N. J. van Druten, and W. Ketterle, Phys. Rev. Lett. **79**, 549 (1997).
[*Eigen 2018*] C. Eigen, J. A. P. Glidden, R. Lopes, E. A. Cornell, R. P. Smith, and Z. Hadzibabic, Nature **563**, 221 (2018).
[*Einstein 1925*] A. Einstein, Sitzungsbericht der Preussichen Akademie der Wissenschaften **1**, 3 (1925).
[*Ensher 1996*] J. R. Ensher, D. S. Jin, M. R. Matthews, C. E. Wieman, and E. A. Cornell, Phys. Rev. Lett. **77**, 4984 (1996).
[*Feng 2019*] L. Feng, J. Hu, L. W. Clark, and C. Chin, Science **363**, 521 (2019).
[*Ferrier-Barbut 2014*] I. Ferrier-Barbut, M. Delehaye, S. Laurent, A. T. Grier, M. Pierce, B. S. Rem, F. Chevy, and C. Salomon, Science **345**, 1035 (2014).
[*Ferrier-Barbut 2016*] I. Ferrier-Barbut, Mixtures of Bose and Fermi Superfluids, PhD thesis, ENS (2016).

[*Fisher 1989*] M. P. A. Fisher, P. B. Weichman, G. Grinstein, and D. S. Fisher, Phys. Rev. B. **40**, 546 (1989).
[*Fletcher 2015*] R. J. Fletcher, M. Robert-de-Saint-Vincent, J. Man, N. Navon, R. P. Smith, K. G. H. Viebahn, and Z. Hadzibabic, Phys. Rev. Lett. **114**, 255302 (2015).
[*Gambassi 2009*] A. Gambassi, J. Phys.: Conf. Ser. **161**, 012037 (2009).
[*Gasparini 2008*] F. M. Gasparini, M. O. Kimball, K. P. Mooney, and M. Diaz-Avila, Rev. Mod. Phys. **80**, 1009 (2008).
[*Gaunt 2013*] A. L. Gaunt, T. F. Schmidutz, I. Gotlibovych, R. P. Smith, and Z. Hadzibabic, Phys. Rev. Lett. **110**, 200406 (2013).
[*Georgescu 2014*] I. M. Georgescu, S. Ashhab, and F. Nori, Rev. Mod. Phys. **86**, 154 (2014).
[*Gerbier 2004*] F. Gerbier, J. H. Thywissen, S. Richard, M. Hugbart, P. Bouyer, and A. Aspect, Phys. Rev. Lett. **92**, 030405 (2004).
[*Giorgini 1996*] S. Giorgini, L. P. Pitaevskii, and S. Stringari, Phys. Rev. A **54**, R4633(R) (1996).
[*Görlitz 2001*] A. Görlitz, J. M. Vogels, A. E. Leanhardt, C. Raman, T. L. Gustavson, J. R. Abo-Shaeer, A. P. Chikkatur, S. Gupta, S. Inouye, T. Rosenband, and W. Ketterle, Phys. Rev. Lett. **87**, 130402 (2001).
[*Greiner 2002*] M. Greiner, O. Mandel, T. Esslinger, T. W. Hänsch, and I. Bloch, Nature **415**, 39 (2002).
[*Grimm 2000*] R. Grimm, M. Weidemüller, and Y. B. Ovchinnikov, Adv. Atom. Mol. Opt. Phys. **42**, 95 (2000).
[*Gross 2011*] N. Gross, Z. Shotan, O. Machtey, S. Kokkelmans, and L. Khaykovich, C. R. Physique **12**, 4 (2011).
[*Gustavson 2002*] T. L. Gustavson, A. P. Chikkatur, A. E. Leanhardt, A. Görlitz, S. Gupta, D. E. Pritchard, and W. Ketterle Phys. Rev. Lett. **88**, 020401 (2002).
[*Hadzibabic 2006*] Z. Hadzibabic, P. Krüger, M. Cheneau, B. Battelier, and J. Dalibard, Nature **441**, 1118 (2006).
[*Hadzibabic 2008*] Z. Hadzibabic, P. Krüger, M. Cheneau, S. P. Rath, and J. Dalibard, New J. Phys. **10**, 045006 (2008).
[*Holthaus 1998*] M. Holthaus, E. Kalinowski, and K. Kirsten, Ann. Phys. **270**, 198 (1998).
[*Horikoshi 2017a*] M. Horikoshi, A. Ito, T. Ikemachi, Y. Aratake, M. Kuwata-Gonokami, M. Koashi, J. Phys. Soc. Jpn. **86**, 104301 (2017).
[*Horikoshi 2017b*] M. Horikoshi, M. Koashi, H. Tajima, Y. Ohashi, and M. Kuwata-Gonokami, Phys. Rev. X **7**, 041004 (2017).
[*Horikoshi 2019*] M. Horikoshi, and M. Kuwata-Gonokami, Int. J. Mod. Phys. E **28**, 1930001 (2019).
[*Howl 2019*] R. Howl, R. Penrose, and I. Fuentes, New J. Phys. **21**, 043047 (2019).
[*Hu 2019*] J. Hu, L. Feng, Z. Zhang, and C. Chin, Nat. Phys. **15**, 785 (2019).
[*Huang 1987*] K. Huang, Statistical Mechanics (John Wiley & Sons, United States, 1987).

[*Huang 2019*] B. Huang, I. Fritsche, R. S. Lous, C. Baroni, J. T. M. Walraven, E. Kirilov, and R. Grimm, Phys. Rev. A **99**, 041602(R) (2019).
[*Ikemachi 2016*] T. Ikemachi, A. Ito, Y. Aratake, Y. Chen, M. Koashi, M. Kuwata-Gonokami, and M. Horikoshi, J. Phys. B: At. Mol. Opt. Phys. **50,** 01LT01 (2016).
[*Inouye 1998*] S. Inouye, M. R. Andrews, J. Stenger, H.-J. Miesner, D. M. Stamper-Kurn, and W. Ketterle, Nature **392**, 151 (1998).
[*Jaksch 1998*] D. Jaksch, C. Bruder, J.I. Cirac, C.W. Gardiner, and P. Zoller, Phys. Rev. Lett. **81**, 3108 (1998).
[*Jin 1996*] D. S. Jin, J. R. Ensher, M. R. Matthews, C. E. Wieman, and E. A. Cornell, Phys. Rev. Lett. **77**, 420 (1996).
[*Jin 1997*] D. S. Jin, M. R. Matthews, J. R. Ensher, C. E. Wieman, and E. A. Cornell, Phys. Rev. Lett. **78**, 764 (1997).
[*Julienne 2014*] P. S. Julienne, and J. M. Hutson, Phys. Rev. A **89**, 052715 (2014).
[*Kocharovsky 2006*] V. V. Kocharovsky, Vl. V. Kocharovsky, M. Holthaus, C. H. R. Ooi, A. A. Svidzinsky, W. Ketterle, and M. O. Scully, Advances in Atomic, Molecular and Optical Physics v. **53**, 291 (2006).
[*Kopietz 2010*] P. Kopietz, L. Bartosch, and F. Schütz, Introduction to the Functional Renormalization Group (Springer, Germany, 2010).
[*Kraemer 2006*] T. Kraemer, M. Mark, P. Waldburger, J. G. Danzl, C. Chin, B. Engeser, A. D. Lange, K. Pilch, A. Jaakkola, H.-C. Nägerl, and R. Grimm, Nature **440**, 315 (2006).
[*Kristensen 2017*] M. A. Kristensen, M. Gajdacz, P. L. Pedersen, C. Klempt, J. F. Sherson, J. J. Arlt, and A. J. Hilliard, J. Phys. B **50**, 034004 (2017).
[*Kristensen 2019*] M. A. Kristensen, M. B. Christensen, M. Gajdacz, M. Iglicki, K. Pawłowski, C. Klempt, J. F. Sherson, K. Rzążewski, A. J. Hilliard, and J. J. Arlt, Phys. Rev. Lett. **122**, 163601 (2019).
[*Ku 2012*] M. J. H. Ku, A. T. Sommer, L. W. Cheuk, and M. W. Zwierlein, Science **335**, 563 (2012).
[*Lamporesi 2013*] G. Lamporesi, S. Donadello, S. Serafini, F. Dalfovo, and G. Ferrari, Nat. Phys. **9**, 656 (2013).
[*Lee 1957*] T. D. Lee, Kerson Huang, and C. N. Yang, Phys. Rev. **106**, 1135 (1957).
[*Leggett 2001*] A. J. Leggett, Rev. Mod. Phys. **73**, 307 (2001).
[*Lepoutre 2016*] S. Lepoutre, L. Fouché, A. Boissé, G. Berthet, G. Salomon, A. Aspect, and T. Bourdel, Phys. Rev. A **94**, 053626 (2016).
[*Lopes 2017*] R. Lopes, C. Eigen, N. Navon, D. Clément, R. P. Smith, and Z. Hadzibabic, Phys. Rev. Lett. **119**, 190404 (2017).
[*Lous 2018*] R. S. Lous, I. Fritsche, M. Jag, F. Lehmann, E. Kirilov, B. Huang, and R. Grimm, Phys. Rev. Lett. **120**, 243403 (2018).
[*Luiten 1996*] O. J. Luiten, M. W. Reynolds, and J. T. M. Walraven, Phys. Rev. A **53**, 381 (1996).

[*Meppelink 2010*] R. Meppelink, R. A. Rozendaal, S. B. Koller, J. M. Vogels, and P. van der Straten, Phys. Rev. A **81**, 053632 (2010).
[*Mewes 1996*] M.-O. Mewes, M. R. Andrews, N. J. van Druten, D. M. Kurn, D. S. Durfee, and W. Ketterle, Phys. Rev. Lett. **77**, 416 (1996).
[*Miesner 1998*] H.-J. Miesner, D. M. Stamper-Kurn, M. R. Andrews, D. S. Durfee, S. Inouye, and W. Ketterle, Science **279**, 1005 (1998).
[*Miyakawa 2000*] T. Miyakawa, T. Suzuki, and H. Yabu, Phys. Rev. A **62**, 063613 (2000).
[*Moerdijk 1995*] A. J. Moerdijk, B. J. Verhaar, and A. Axelsson, Phys. Rev. A **51**, 4852 (1995).
[*Mølmer 1998*] K. Mølmer, Phys. Rev. Lett. **80**, 1804 (1998).
[*Mordini 2020*] C. Mordini, D. Trypogeorgos, A. Farolfi, L. Wolswijk, S. Stringari, G. Lamporesi, and G. Ferrari, Phys. Rev. Lett. **125**, 150404 (2020).
[*Morgan 2000*] S. A. Morgan, J. Phys. B: At. Mol. Opt. Phys. **33**, 3847 (2000).
[*Morsch 2006*] O. Morsch and M. Oberthaler, Rev. Mod. Phys. **78**, 179 (2006).
[*Myatt 1997*] C. J. Myatt, E. A. Burt, R. W. Ghrist, E. A. Cornell, and C. E. Wieman, Phys. Rev. Lett. **78**, 586 (1997).
[*Napiorkowski 2013*] M. Napiorkowski, P. Jakubczyk, and K. Nowak, J. Stat. Mech. 06015 (2013).
[*Nascimbène 2010*] S. Nascimbène, N. Navon, F. Chevy, and C. Salomon, New J. Phys. **12** 103026 (2010).
[*Navez 1997*] P. Navez, D. Bitouk, M. Gajda, Z. Idziaszek, and K. Rzążewski, Phys. Rev. Lett. **79**, 1789 (1997).
[*Navon 2011*] N. Navon, S. Piatecki, K. Günter, B. Rem, T. C. Nguyen, F. Chevy, W. Krauth, and C. Salomon, Phys. Rev. Lett. **107**, 135301 (2011).
[*Navon 2015*] N. Navon, A. L. Gaunt, R. P. Smith, and Z. Hadzibabic, Science **347**, 167 (2015).
[*Nguyen 2019*] J. H. V. Nguyen, M. C. Tsatsos, D. Luo, A. U. J. Lode, G. D. Telles, V. S. Bagnato, and R. G. Hulet, Phys. Rev. X **9**, 011052 (2019).
[*O'Hara 2001*] K. M. O'Hara, M. E. Gehm, S. R. Granade, and J. E. Thomas, Phys. Rev. A **64**, 051403 (2001).
[*Pathria 2011*] R.K. Pathria and P. D. Beale, Statistical Mechanics (Academic Press, United States, 2011).
[*Pelissetto 2002*] A. Pelissetto, and E. Vicari, Phys. Rept. **368**, 549 (2002).
[*Penrose 1956*] O. Penrose and L. Onsager, Phys. Rev. **104**, 576 (1956).
[*Pérez-García 1997*] V. M. Pérez-García, H. Michinel, J. I. Cirac, M. Lewenstein, and P. Zoller, Phys. Rev. A **56**, 1424 (1997).
[*Petrov 2000*] D. S. Petrov, G. V. Shlyapnikov, and J. T. M. Walraven, Phys. Rev. Lett. **85**, 3745 (2000).
[*Pietraszewicz 2017*] J. Pietraszewicz, E. Witkowska, and P. Deuar, Phys. Rev. A **96**, 033612 (2017).

[*Politzer 1996*] H. D. Politzer, Phys. Rev. A **54**, 5048 (1996).
[*Pollack 2009*] S. E. Pollack, D. Dries, M. Junker, Y. P. Chen, T. A. Corcovilos, and R. G. Hulet, Phys. Rev. Lett. **102**, 090402 (2009).
[*Poveda-Cuevas 2015*] F. J. Poveda-Cuevas, P. C. M. Castilho, E. D. Mercado-Gutierrez, A. R. Fritsch, S. R. Muniz, E. Lucioni, G. Roati, and V. S. Bagnato, Phys. Rev. A **92**, 013638 (2015).
[*Proukakis 2008*] N. P. Proukakis, and B. Jackson, J. Phys. B: At. Mol. Opt. Phys. **41**, 203002 (2008).
[*Ramanathan 2012*] A. Ramanathan, S. R. Muniz, K. C. Wright, R. P. Anderson, W. D. Phillips, K. Helmerson, and G. K. Campbell, Rev. Sci. Instrum. **83**, 083119 (2012).
[*Rasolt 1984*] M. Rasolt, M. J. Stephen, M. E. Fisher, and P. B. Weichman, Phys. Rev. Lett. **53**, 798 (1984).
[*Reyes-Ayala 2019*] I. Reyes-Ayala, F. J. Poveda-Cuevas, and V. Romero-Rochin, J. Stat. Mech. 113102 (2019).
[*Roati 2008*] G. Roati, C. D'Errico, L. Fallani, M. Fattori, C. Fort, M. Zaccanti, G. Modugno, M. Modugno, and M. Inguscio, Nature **453**, 895 (2008).
[*Roy 2017*] R. Roy, A. Green, R. Bowler, and S. Gupta, Phys. Rev. Lett. **118**, 055301 (2017).
[*Schmitt 2014*] J. Schmitt, T. Damm, D. Dung, F. Vewinger, J. Klaers, and M. Weitz, Phys. Rev. Lett. **112**, 030401 (2014).
[*Schreck 2001a*] F. Schreck, L. Khaykovich, K. L. Corwin, G. Ferrari, T. Bourdel, J. Cubizolles, and C. Salomon, Phys. Rev. Lett. **87**, 080403. (2001).
[*Schreck 2001b*] F. Schreck, G. Ferrari, K. L. Corwin, J. Cubizolles, L. Khaykovich, M.-O. Mewes, and C. Salomon, Phys. Rev. A **64**, 011402(R) (2001).
[*Sethna 2006*] J. P. Sethna, Statistical Mechanics: Entropy, Order Parameters and Complexity (Oxford University Press, England, 2006).
[*Shiozaki 2014*] R. F. Shiozaki, G. D. Telles, P. Castilho, F. J. Poveda-Cuevas, S. R. Muniz, G. Roati, V. Romero-Rochin, and V. S. Bagnato, Phys. Rev. A **90**, 043640 (2014).
[*Smith 2011*] R. P. Smith, R. L. D. Campbell, N. Tammuz, and Z. Hadzibabic, Phys. Rev. Lett. **106**, 250403 (2011).
[*Smith 2016*] R. P. Smith, arXiv:1609.04762 (2016).
[*Srednicki 1994*] M. Srednicki, Phys. Rev. E **50**, 888 (1994).
[*Stanley 1999*] H. E. Stanley, Rev. Mod. Phys. **71**, S358 (1999).
[*Strecker 2002*] K. E. Strecker, G. B. Partridge, A. G. Truscott, and R. G. Hulet, Nature **417**, 150 (2002).
[*Svidzinsky 2018*] A. Svidzinsky, M. Kim, G. Agarwal and Marlan O Scully, New J. Phys. **20**, 013002 (2018).
[*Szczepkowski 2009*] J. Szczepkowski, R. Gartman, M. Witkowski, L. Tracewski, M. Zawada, and W. Gawlik, Rev. Sci. Instrum. **80**, 053103 (2009).
[*Takeuchi 2010*] K. A. Takeuchi, and M. Sano, Phys. Rev. Lett. **104**, 230601 (2010).

[*Takeuchi 2011*] K. A. Takeuchi, M. Sano, T. Sasamoto, and H. Spohn, Sci. Rep. **1**, 34 (2011).
[*Tammuz 2011*] N. Tammuz, R. P. Smith, R. L. D. Campbell, S. Beattie, S. Moulder, J. Dalibard, and Z. Hadzibabic, Phys. Rev. Lett. **106**, 230401 (2011).
[*Tarasov 2014*] S. V. Tarasov, Vl. V. Kocharovsky, and V. V. Kocharovsky, Phys. Rev. A **90**, 033605 (2014).
[*Touchette 2015*] H. Touchette, J. Stat. Phys. **159**, 987 (2015).
[*Truscott 2001*] A. G. Truscott, K. E. Strecker, W. I. McAlexander, G. B. Partridge, and R. G. Hulet, Science **291**, 2570 (2001).
[*Weichman 1986*] P. B. Weichman, M. Rasolt, M. E. Fisher, and M. J. Stephen, Phys. Rev. B. **33**, 4632 (1986).
[*Weiler 2008*] C. N. Weiler, T. W. Neely, D. R. Scherer, A. S. Bradley, M. J. Davis, and B. P. Anderson, Nature **455**, 948 (2008).
[*Wigley 2016*] P. B. Wigley, P. J. Everitt, K. S. Hardman, M. R. Hush, C. H. Wei, M. A. Sooriyabandara, P. Manju, J. D. Close, N. P. Robins, and C. C. N. Kuhn, Opt. Lett. **41**, 4795 (2016).
[*Yao 2016*] X. –C. Yao, H. -Z. Chen, Y. –P. Wu, X. –P. Liu, X. –Q. Wang, X. Jiang, Y. Deng, Y. –A. Chen, and J. –W. Pan, Phys. Rev. Lett. **117**, 145301 (2016).
[*Yukalov 2016*] V.I. Yukalov, Laser Phys. **26**, 062001(2016).
[*Zagrebnov 2001*] V.A. Zagrebnov, J. B. Bru, Phys. Rep. **350**, 291 (2001).
[*Zannetti 2015*] M. Zannetti, EPL **111**, 20004 (2015).
[*Zhang 2020*] Z. Zhang, K.-X. Yao, L. Feng, J. Hu, and C. Chin, Nat. Phys. 16, 652 (2020).
[*Zurek 1996*] W. H. Zurek, Phys. Rep. **276**, 177 (1996).

Acknowledgements

The research presented in this thesis was conducted during my Doctor's course in the Gonokami-Yumoto-Ideguchi Group within the Department of Physics, Graduate School of Science in the University of Tokyo. I am honored to have had the opportunity to work in such a professional, active, and friendly group. The abundant diversity in research directions present in the group provided me unique opportunity to access different field of researches. I believe that the knowledge and the way of scientific thinking I learnt during my years in the University of Tokyo will provide me great guidance in the future.

It has been a great privilege to work with Prof. Kosuke Yoshioka, Prof. Makoto Kuwata-Gonokami, Prof. Junji Yumoto and Prof. Takuro Ideguchi.

I must thank my supervisor, Prof. Yoshioka, for overseeing my research while being extremely busy operating his own group. He provided me great help in my experimental direction with his keen vision. I am deeply appreciative of his detailed suggestions to the creation of this thesis. I must also thank him for giving me unforsaken advices and encouragements during this unusual year.

Prof. Gonokami, despite being busy as the head of the University, has been actively engaged in the research conducted in the group. I am really surprised at his vast knowledge across a wide field of researches and his ability to give useful and precise advices. I am especially grateful for his advice on how I should interpret the result of this thesis.

I would like to send my most sincere gratitude to my direct overseer, Dr. Munekazu Horikoshi. He provided me countless help during my experiments with his advanced know-how and outstanding skills. Without his crucial advices on data processing, the work in this thesis cannot be done. Congratulations on his new job as professor! I wish Horikoshi-san every success in his new position.

Though not directly involved in my research, I appreciate the friendliness of Prof. Yumoto and Prof. Ideguchi. The life stories of Prof. Yumoto have always been enjoyable and Prof. Ideguchi's knowledge towards pop culture sparked many delightful conversations.

I shall also thank the group staffs for providing me with accurate information and timing suggestions. They had made my life much easier.

The rest adorable members of the group deserve a heartful thanks for being productive colleagues and good friends. They were indispensable for my pleasant years at the University of Tokyo.